Remote Sensing of Environment xxx (2009) xxx–xxx

Contents lists available at ScienceDirect

Remote Sensing of Environment

journal homepage: www.elsevier.com/locate/rse

Remote sensing of mineral dust over land with MSG infrared channels: A new Bitemporal Mineral Dust Index

L. Klüser [a,b,*], K. Schepanski [c,d]

[a] German Aerospace Center (DLR), German Remote Sensing Data Center (DFD), Weßling, Germany
[b] University of Augsburg, Institute of Physics, Augsburg, Germany
[c] Leibniz Institute for Tropospheric Research (IfT), Leipzig, Germany
[d] Leibniz Institute of Marine Sciences, IFM-GEOMAR, Kiel, Germany

ARTICLE INFO

Article history:
Received 17 October 2008
Received in revised form 14 April 2009
Accepted 17 April 2009
Available online xxxx

Keywords:
Mineral dust
Aerosol
MSG

ABSTRACT

A new Bitemporal Mineral Dust Index (BMDI) is derived from Meteosat Second Generation (MSG) infrared observations over land at two different time slots per day.

This daily dust index is evaluated with AErosol RObotic NETwork (AERONET) surface observations, MODerate resolution Imaging Spectro-radiometer (MODIS) "Deep Blue" Aerosol Optical Depth (AOD) and Ozone Monitoring Instrument (OMI) Aerosol Index, showing a good capability of the BMDI for dust detection and dust load estimation over land and also over deserts. BMDI dust detection is shown to be limited in scenes with high atmospheric humidity as e.g. coastal regions. In particular the insensitivity of BMDI to biomass burning aerosol is shown, leading to the possibility of remote sensing of mineral dust also in regions with large contributions of biomass burning aerosol to the total column aerosol concentrations. Time series of mineral dust as inferred from BMDI for the year 2006 are presented for four regions over the Sahara. These time series show strong (and different) annual cycles of dust load for all four regions. Especially the strong episodic character of atmospheric dust in the main source regions can be inferred from BMDI observations.

1. Introduction

Mineral dust has been reported to have many effects on the climate system, e.g. radiative effects reducing surface insolation (e.g. King et al., 1999; Slingo et al., 2006) and interactions with cloud microphysics (e.g. Mahowald & Kiehl, 2003; Ansmann et al., 2008), leading to precipitation suppression in the Sahel (e.g. Rosenfeld et al., 2001; Hui et al., 2008). Mineral dust transport over the Atlantic Ocean (e.g. Prospero & Carlson, 1980) is also assumed to affect tropical storm intensities (Dunion & Velden, 2004; Evan et al., 2006) and is a major source of iron for the Atlantic Ocean (Jickells et al., 2005; Mahowald et al., 2005) and the Amazon rainforest (Koren et al., 2006). Moreover solar energy industries are highly sensitive to the presence of mineral dust aerosols (Breitkreuz et al., 2007), especially in the Mediterranean region, where dust outbreaks are quite common (Barkan et al., 2005; Meloni et al., 2006).

Thus there is a strong interest in mineral dust detection and dust load estimation from satellite observations. Efforts have been made to detect mineral dust not only over dark surfaces or ocean, where aerosol optical depth (AOD) retrievals from reflected solar radiation often are confined to, but also over the inland source regions within the large deserts such as the Sahara. Those estimates of atmospheric dust load are mostly observations in shortwave (blue to ultraviolet) or thermal infrared (IR) wavelength bands. Examples of shortwave algorithms are: the Ozone Monitoring Instrument (OMI, onboard the Aura satellite) Absorbing Aerosol Index (AI, Torres et al., 1998), the "Deep Blue" algorithm (Hsu et al., 2004) for observations of the MODerate resolution Imaging Spectro-radiometer (MODIS) flying onboard the Terra and Aqua satellites and the SYNergetic AErosol Retrieval SYNAER from ENVISAT observations (Holzer-Popp et al., 2008). At the present time, these algorithms are only applied to instruments onboard polar orbiting satellites due to the availability of appropriate spectral bands. Another approach to detect mineral dust over deserts is to exploit thermal infrared channels, which are also available on geostationary satellites and thus allow for daily or sub-daily dust observations in the field-of-view (FOV) of the satellite. IR observations over land are used in a number of methods of remote sensing of mineral dust over land, for example, the Infrared Difference Dust Index (IDDI) described by Brooks and Legrand (2006) and Legrand et al. (2001), and for dust detection and AOD retrieval (Li et al., 2007). In addition Chaboureau et al. (2007) use IR observations for estimating the diurnal cycle of mineral dust in Africa. Schepanski et al. (2007) and Schepanski et al. (in press) use IR observations from the Meteosat Second Generation (MSG) Spinning Enhanced Visible and InfraRed Imager (SEVIRI) instrument compiled to appropriate Red–Green–Blue (RGB) composite images of

---

* Corresponding author. German Aerospace Center (DLR), German Remote Sensing Data Center (DFD), Weßling, Germany.
E-mail address: lars.klueser@dlr.de (L. Klüser).

0034-4257/$ – see front matter © 2009 Elsevier Inc. All rights reserved.
doi:10.1016/j.rse.2009.04.012

Please cite this article as: Klüser, L., & Schepanski, K., Remote sensing of mineral dust over land with MSG infrared channels: A new Bitemporal Mineral Dust Index, *Remote Sensing of Environment* (2009), doi:10.1016/j.rse.2009.04.012

brightness temperature differences (BTD) to detect and characterise dust source areas concerning their spatio-temporal variability. The paper is structured as follows: an overview over infrared remote sensing of mineral dust is given in Section 2, followed by an introduction of the new developed Bitemporal Mineral Dust Index (BMDI) and a detailed description of the presented algorithm together with an evaluation of sensitivities and limitations during an episode of Sahara-wide dust activity in Section 3. In Section 4 the comparison of one year of BMDI observations with aerosol observations from the Aerosol Robotic Network (AERONET), MODIS “Deep Blue” AOD and OMI AI is presented and evaluated.

Section 5 exemplarily describes the annual cycle of mineral dust as inferred from BMDI observations for some source areas, followed by summarising and concluding remarks in Section 6.

2. Infrared remote sensing of mineral dust

Besides the need for accurate cloud screening, space-borne detection of mineral dust over land is additionally complicated by completely different surface characteristics regarding to its emissivity and absorption at different wavelength bands as well as by absorption of the atmospheric constituents like water vapour and the inhomogeneity of dust properties itself. A dust detection strategy which does not depend on a priori information or climatologies has to account for such variations of properties.

One method to detect mineral dust from IR radiation is the Infrared Difference Dust Index (IDDI) developed for observations of the first generation METEOSAT satellites (Brooks & Legrand, 2006; Legrand et al., 2001). In this method the highest value of the METEOSAT thermal IR channel brightness temperatures of a 15 days reference period is assumed to represent background conditions. The dust load is estimated by the difference between the observed brightness temperature and the background assumption. Stationarity of surface temperatures is assumed for the reference period, which is stated to be a compromise between a period long enough to cover dust-free conditions and short enough to legitimate the stationarity assumption. Especially during very strong or prolonged dust events this assumption can be invalid (Brooks & Legrand, 2006; King et al., 1999), resulting in a significant over- or underestimation of the atmospheric dust load.

A similar approach for the detection of mineral dust with MSG–SEVIRI observations is described in Li et al. (2007). Those authors compare brightness temperatures of the 10.8 μm channel ($T_{10.8}$) with respective brightness temperatures from the last dust-free day prior to the observation for dust detection. $\mathrm{AOD}_{0.55}$ is calculated for dusty scenes based on $T_{10.8}$ due to a quasi-linear relationship between $T_{10.8}$ and $\mathrm{AOD}_{0.55}$. Furthermore, Li et al. (2007) retrieve the effective particle radius from the split-window brightness temperature difference (BTD)

$$\mathrm{BTD} = T_{10.8} - T_{12.0} \tag{1}$$

which depends on the dust load and the particle size (Chaboureau et al., 2007; Li et al., 2007).

BTD described by Eq. (1) is often used for dust detection (e.g. Pierangelo et al., 2004; Chaboureau et al., 2007; Schepanski et al., 2007), but in most cases with restrictions regarding to the atmospheric dust load (Chaboureau et al., 2007; Li et al., 2007). Furthermore one should be aware, that the atmospheric water vapour also has an impact on the BTD (e.g. Dunion & Velden, 2004; Chaboureau et al., 2007; Schroedter-Homscheidt et al., 2008), which is in contrast to the dust effect. Thus dust in a dry environment is more likely to be detected by means of BTD than dust in an environment of high humidity (see e.g. Dunion & Velden, 2004; Chaboureau et al., 2007).

As the first generation METEOSAT satellites lack the availability of two split-window IR channels, Legrand et al. (2001) and also Miller et al. (2008) could not use the benefits of BTD for dust detection.

The spectral extinction coefficient of mineral dust shows a significant local maximum at about 10 μm (Pierangelo et al., 2004; Chaboureau et al., 2007) resulting in higher absorption of radiation and thus reduced $T_{10.8}$ compared to $T_{12.0}$ brightness temperatures (Ackerman, 1997; Sokolik, 2002, Chaboureau et al., 2007). The spectral signature of extinction by mineral dust would strongly motivate the utilisation of 8.7 μm and 9.7 μm SEVIRI observations for dust detection, but ozone absorption at 9.7 μm (Schmetz et al., 2002) and high temporal and spatial variability of surface emissions at wavelengths below 10 μm (Ogawa et al., 2003; Li et al., 2007) as well as a strong influence of water vapour at 8.7 μm prevent those channels from being useful for reliable dust detection.

Despite those restrictions $T_{8.7}$ observations are used for the generation of “dust” scheme RGB images as used e.g. in Knippertz et al. (2008) and Schepanski et al. (2007) for visual dust detection.

Over land, especially in tropical and subtropical regions, surface temperatures show a significant diurnal cycle with high amplitudes, provided that no clouds are present (e.g. King et al., 1999). This diurnal cycle is represented by the (cloud-free) brightness temperatures observed by satellite instruments. Also the split-window BTD is affected by the diurnal cycle, as due to spectral emissivity variations (Ogawa et al., 2003) and the atmospheric water vapour content (Schroedter-Homscheidt et al., 2008) the temperature amplitude is not exactly the same at both wavelengths. Within the boundary layer, airborne mineral dust itself shows patterns of a diurnal cycle, controlled by the boundary layer dynamics (Schepanski et al., in press).

However, the amplitude of this diurnal cycle shows a very high spatial variability (Engelstaedter et al., 2006). Engelstaedter et al. (2006), Chaboureau et al. (2007) and Schepanski et al. (in press), all show a daily minimum in dust mobilisation in the Sahara and Sahel region between 21:00 and 03:00 UTC and a corresponding mobilisation maximum between 06:00 and 15:00 UTC.

Observations of Saharan dust emissions based on 15-minute MSG observations indicate morning hours as time of day with most frequently observed dust sources activations (Schepanski et al., submitted for publication). 65% of Saharan dust events start during 06:00–09:00 UTC (based on the observation period Mar 2006–Aug 2008). Meteorological observations from weather stations as well as regional and global models point towards an important role of the breakdown of the nocturnal low-level jet (LLJ) during the morning hours. The nocturnal LLJ, defined by a low-level wind speed maximum at around 1–1.5 km height (e.g. Blackadar, 1957; Holton, 1967; Banta et al., 2006), results from a frictional decoupling of elevated air layers from the surfaces and near surface layers due to nighttime stratification. With increasing insolation during the morning hours, convective turbulence increases, the air aloft is coupled to the surface air layers and the LLJ's momentum is mixed downward leading to suddenly increasing surface wind speeds (Kalu, 1979; Lenschow & Stankov, 1979; Schepanski et al., in press). Dust mobilisation in case of wind speeds exceeding local thresholds for dust emission depends on soil texture (Marticorena & Bergametti, 1995). During day time, airborne dust is distributed homogeneously over the entire boundary layer (BL). With dawn, BL turbulence ceases and atmospheric stratification increases. Airborne dust within stratified layers near the surface tends to deposit due to gravitational settling. Dust within the residual BL will be transported within the geostrophic flow (Kalu, 1979; Schepanski et al., 2009). During the next day, the dust layer will be coupled to the developing daytime BL, assumed that the BL depth reaches the height of the dust layer (e.g. Kalu, 1979).

3. Description of the index

3.1. Motivation and Bitemporal Mineral Dust Index Definition

The diurnal cycle of both dust mobilisation and land surface temperatures can be utilised to detect mineral dust over land from

Please cite this article as: Klüser, L., & Schepanski, K., Remote sensing of mineral dust over land with MSG infrared channels: A new Bitemporal Mineral Dust Index, *Remote Sensing of Environment* (2009), doi:10.1016/j.rse.2009.04.012

day- and nighttime MSG–SEVIRI observations without restrictions due to the background albedo. Thus airborne dust detection is possible also over bright desert surfaces.

The difference of $T_{10.8}$ between night and day is reduced in the presence of dust due to extinction of IR radiation at 10.8 µm combined with a reduction of daytime surface temperatures by the dust optical depth in the solar spectral range (Brooks & Legrand, 2006). Thus the difference

$$\Delta T_{10.8} = T_{10.8}(\mathrm{day}) - T_{10.8}(\mathrm{night}) \quad (2)$$

is influenced by the atmospheric column dust load and can be used for dust detection. If no clouds are present at both observation times, a lower value of $\Delta T_{10.8}$ can be regarded as an indicator for a higher dust load. The theory behind this approach is similar to Legrand et al. (2001) and Li et al. (2007), but differing in the point that observations at different times of the day are used instead of observations of a fixed time on different days.

Of course, $\Delta T_{10.8}$ is not only sensitive to the presence of mineral dust, but is also a product of the meteorological conditions, regional surface temperatures and surface emissivity and atmospheric moisture (see e.g. Legrand et al., 2001 for a discussion of the influence of water vapour on infrared observations by satellites). For the March 7, 2006 Sahara dust storm presented in Fig. 1 (a detailed description of this dust event is given in Tulet et al., 2008) the resulting $\Delta T_{10.8}$ is shown in Fig. 2c. The strong reduction of $\Delta T_{10.8}$ by the presence of mineral dust (as indicated by Fig. 1) is clearly evident, also a reduction of $\Delta T_{10.8}$ by the moist air south of the Intertropical Discontinuity (ITD) in the southern Sahel domain. Especially in the south-eastern part of the Sahara terrain structures can be recognized in $\Delta T_{10.8}$, indicating the strong influence of the surface temperatures on the night-to-day difference of $T_{10.8}$. These terrain structures are no longer evident in this image in regions of airborne dust, but of course also here $\Delta T_{10.8}$ is modulated by the meteorological conditions. Furthermore the reduction effect of mineral dust on the IR brightness temperature is a function of both column aerosol load and dust layer height. Very low $\Delta T_{10.8}$ as it is present in Fig. 2c in the Western Sahara represents very high dust loads together with high elevations of the dust layer, while both lower dust load and lower dust layer altitudes lead to higher $\Delta T_{10.8}$ values.

Thus $\Delta T_{10.8}$ can help to improve dust detection and qualitative estimation of the atmospheric dust load, but is of limited use for dust load retrieval without assumptions on the background conditions or additional information.

It should be noted that the lack of high surface temperature variation over ocean prevents this method from being applied over ocean surfaces.

As described above, the split-window brightness temperature difference (Eq. (1)) can be used for remote sensing of airborne mineral dust.

Due to the peak of extinction at around 10 µm, BTD is low or negative in the presence of atmospheric mineral dust (Sokolik, 2002; Pierangelo et al., 2004, Chaboureau et al., 2007) and is increased in environments of high humidity (Chaboureau et al., 2007). Thus, low daytime BTD represents dry and dusty air, while high daytime BTD represents no dust or humid air with low dust concentrations, where the humidity effect onto the BTD masks the dust effect. In the presence of very high dust loads, BTD can get saturated due to the strong extinction within the dust layer. Thus, the minimum BTD does not necessarily reflect maximum dust load, but merely moderate dust load, while very high dust loads are represented by only slightly negative BTD. It follows, that BTD alone is not suitable for proper mineral dust detection and estimation of the atmospheric dust load.

During nighttime the dust load often is lower and the height of aged dust layers decreases due to the subsidence induced by the surface cooling.

From radiation transfer considerations also follows a reduction of BTD with increasing surface temperatures in the presence of mineral dust for moderate dust load. With assumed stationary dust load the daytime BTD would then be lower than the nighttime BTD. Consequently, mineral dust effects are more pronounced in daytime BTD observations than in nighttime observations. Fig. 2a and b shows the BTD of the March 7, 2006 dust storm at 03:00 UTC and 12:00 UTC respectively. Regions with mineral dust are generally characterised by negative BTD, while in regions with higher humidity BTD is increased (e.g. in the North African coast of the Mediterranean Sea and in the southern Sahel domain). Due to the effects described above, BTD reaches lower negative values at 12:00 UTC than at 03:00 UTC.

Thus the difference between day- and nighttime BTD observations can also be applied for dust detection:

$$\Delta BTD = BTD\,(\mathrm{day}) - BTD\,(\mathrm{night}). \quad (3)$$

Again, this difference is a product of several environmental factors such as surface temperatures and emissivity, atmospheric moisture,

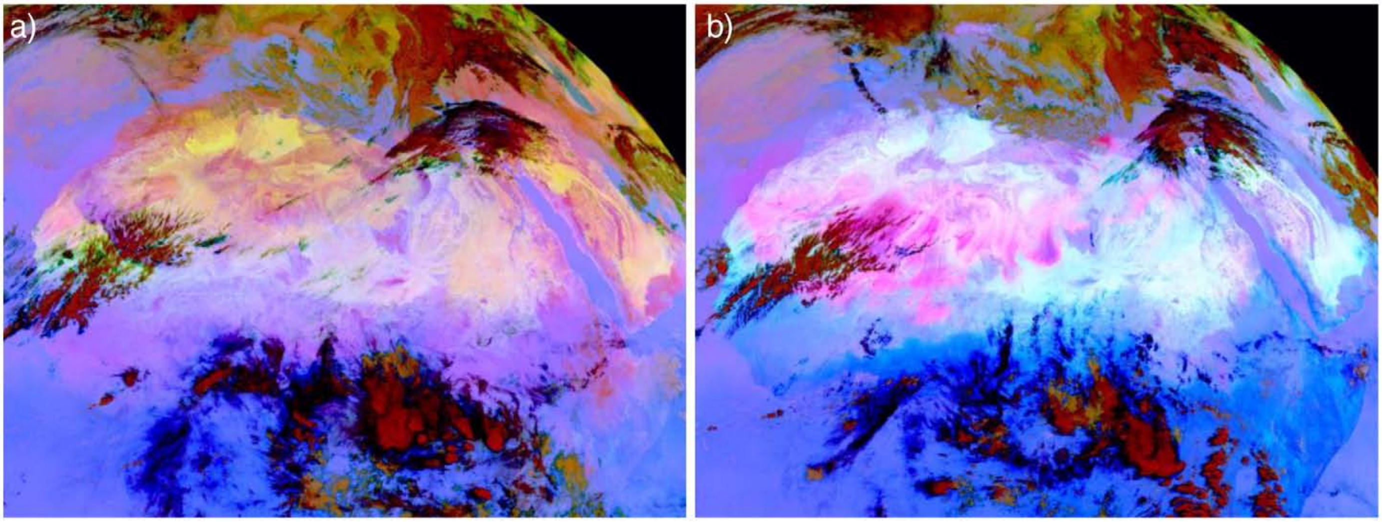

Fig. 1. The March 7, 2006 dust storm at 03:00 UTC (a) and 12:00 UTC (b). In the "MSG dust" RGB colour scheme used here the red channel represents $T_{12.0}$–$T_{10.8}$, the green channel represents $T_{10.8}$–$T_{8.7}$ and the blue channel represents $T_{10.8}$ (inverted). (For interpretation of the references to colour in this figure legend, the reader is referred to the web version of this article.)

Please cite this article as: Klüser, L., & Schepanski, K., Remote sensing of mineral dust over land with MSG infrared channels: A new Bitemporal Mineral Dust Index, *Remote Sensing of Environment* (2009), doi:10.1016/j.rse.2009.04.012

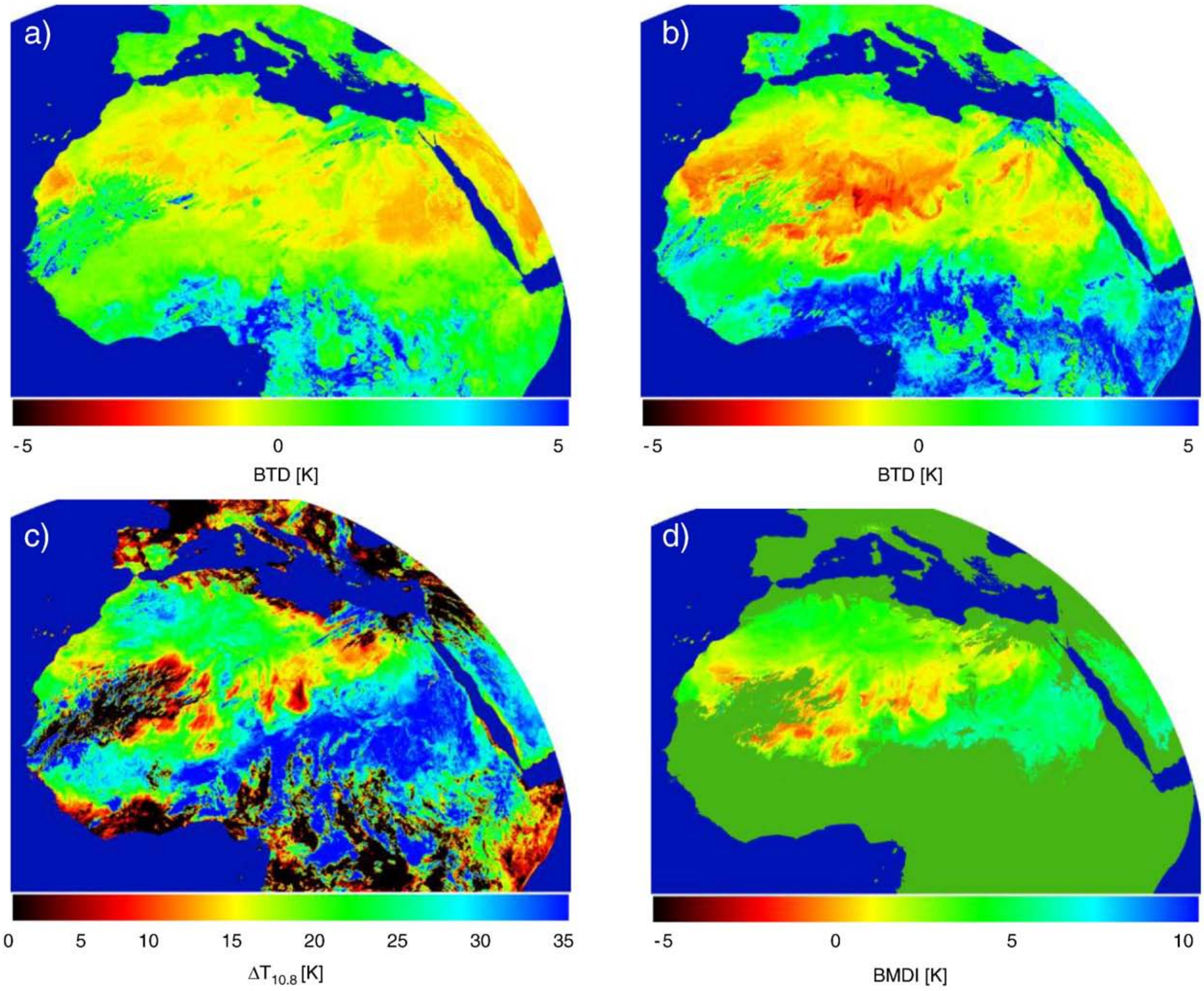

Fig. 2. The 07.03.2006 dust storm: BTD for 03:00 UTC (a) and for 12:00 UTC (b), $\Delta T_{10.8}$ (c) and the resulting BMDI for cloud-free pixels having passed the tests in Eqs. (4) and (5) (d). Low BMDI values indicate high dust loads.

dust layer height and dust concentrations. Thus ΔBTD alone has limitations for dust load retrieval, which is generally true for BTD observations. But nonetheless, ΔBTD is very useful for dust detection, as can be seen in the example in Fig. 2a and b.

As a result of the predominant dust source activation times described in Schepanski et al. (in press), the 03:00 UTC slot for nighttime observations and the 12:00 UTC slot for daytime observations are selected for the whole MSG FOV.

Although at both 03:00 UTC and 12:00 UTC slots, the assumption of minimum and maximum dust source activity (see Section 2) and also that of minimum and maximum surface temperatures at those fixed time observation times are obviously not valid all over the MSG FOV, those observation times work quite well for large parts of the MSG FOV. The advantage of looking onto the whole FOV at the same times outweighs the disadvantage of not exactly meeting minimum and maximum time slots for dust activation and temperatures and thus justifies the selected observation timeslots. But of course one should be aware, that e.g. on the Arabian peninsula 03:00UTC means approximately 06:00 local time. Thus in this part of the FOV the observation times represent morning and afternoon hours instead of really giving the night–day contrast.

The described effects for both $\Delta T_{10.8}$ and ΔBTD are only valid in cloud-free atmospheres, as clouds can have similar or very different effects onto those observations. Thus the first step of every dust detection algorithm is cloud screening.

In our method, clouds are detected by the Avhrr Processing scheme Over Land, cLouds and Ocean (APOLLO) described in Kriebel et al. (2003) in an adaption to MSG.

Furthermore it is highly evident from Fig. 2, that not all regions with low $\Delta T_{10.8}$ and low BTD differences show mineral dust. Thus some additional thresholds are necessary for filtering scenes which are more likely to show mineral dust than others.

This pre-filtering of dust-likelihood is achieved by the following thresholds:

$$\begin{array}{lcr} T_{10.8}(03:00) & \geq & 273\,\mathrm{K} \\ \mathrm{BTD}(03:00) & < & 1\,\mathrm{K} \end{array} \tag{4}$$

for nighttime observations and

$$\begin{array}{lcr} T_{10.8}(12:00) & \geq & 273\,\mathrm{K} \\ \mathrm{BTD}(12:00) & < & 0\,\mathrm{K} \end{array} \tag{5}$$

for daytime observations.

By the restriction to scenes with day- and nighttime $T_{10.8}$ greater than 273 K effects of snowy scenes and glaciers are avoided, which show very low deviations between day- and nighttime values of $T_{10.8}$ and BTD. Additionally, the BTD thresholds are used to separate dusty scenes from scenes with low deviations occurring due to the meteorological conditions rather than to the presence of airborne dust. The slightly higher BTD threshold for nighttime observations

Please cite this article as: Klüser, L., & Schepanski, K., Remote sensing of mineral dust over land with MSG infrared channels: A new Bitemporal Mineral Dust Index, *Remote Sensing of Environment* (2009), doi:10.1016/j.rse.2009.04.012

results from the different effects onto nighttime BTD described above. From Fig. 2a and b can be seen, that BTD values in dusty regions are well below the BTD thresholds given here. This has been tested with several other dust episodes during all seasons (not shown).

Limb darkening effects affect IR observations at high viewing zenith angles by extinction due to the long optical path through the atmosphere (Minnis et al., 1991), leading to reduced radiance in the limb regions. These effects can be avoided by restricting the application of IR dust detection to viewing zenith angles lower than 60°.

In order to present a comparable value range of the resulting dust index, the observations of $\Delta T_{10.8}$ are confined to the interval [0 K, 35 K] and BTD values lower than −5 K are treated as being −5 K. As the range of $\Delta T_{10.8}$ is much greater than the BTD ranges, this observation is divided by the empirical value of 7 for a similar weighting of both observations (compare the BTD and $\Delta T_{10.8}$ values in Fig. 2). For cloud-free MSG pixels having passed the tests and restrictions described above, the Bitemporal Mineral Dust Index (BMDI) then is the sum of ΔBTD and the weighted $\Delta T_{10.8}$:

$$\mathrm{BMDI} = \Delta BTD + \frac{1}{7}\Delta T_{10.8}. \tag{6}$$

As airborne dust is represented by low $\Delta T_{10.8}$ and low or negative ΔBTD, low BMDI values represent high mineral dust loads. Due to the influence of several environmental factors on both $\Delta T_{10.8}$ and ΔBTD, this dust index is only semi-quantitative and BMDI values are not linearly related to dust loads. Especially the influence of water vapour on $\Delta T_{10.8}$, ΔBTD and also the threshold tests in the pre-filtering (Eqs. (4) and (5)) is assumed to have large impacts on both BMDI values and overall detectability of dust in environments with high humidity (see also Legrand et al., 2001 for limitations of IR dust detection due to water vapour effects).

The possible range of the BMDI is given by the interval [−5 K, 10 K]. The BMDI for the Sahara dust storm of March 7, 2006 is shown in Fig. 2d. The areas with high dust loads are characterised by negative BMDI values, low positive BMDI values represent areas with moderate dust load.

3.2. Sensitivity to mineral dust and other aerosols

Both Rudich et al. (2003) and Klüser et al. (2008) show a significant reduction of surface temperatures over the Middle East deserts due to absorption of solar radiation by smoke aerosol. As the BMDI is designed to detect mineral dust aerosol only, $T_{10.8}$ solely seems not to be suitable to distinguish between mineral dust and other aerosol species in regions, where optically thick aerosol plumes can occur, e.g. in the West-African Monsoon region (King et al., 1999). Kaufman and Fraser (1997) show significant absorption of solar radiation by biomass burning aerosols in Amazonia, leading to a stabilisation of the boundary layer and reduced surface temperatures as described e.g. in Klüser et al. (2008). As smoke plumes do not influence BTD by extinction (see e.g. Ackerman, 1997) but only by the reduction of surface temperatures, BTD is only very weakly affected by smoke plumes (Pierangelo et al., 2004).

Indeed, for the smoke event over Middle Eastern deserts described in Klüser et al. (2008), in the areas of decreased surface temperatures below the smoke plume BTD values are increased above the thresholds of the BMDI pre-filtering of Eq. (5) (not shown). This increase of BTD values due to the decrease of surface temperatures is consistent with the argumentation given above for surface temperature influences onto ΔBTD. Thus, while $\Delta T_{10.8}$ and ΔBTD would be reduced by smoke plumes in the same way as by mineral dust due to the daytime surface cooling, the BTD thresholds in the pre-filtering prevent smoke plumes from being recognized as mineral dust.

Due to the incorporation of two MSG observation times with a delay of 9 hours, BMDI values are the result of column dust load, and atmospheric and surface conditions at both observation times.

Several external parameters besides the column particle concentration impact on the BMDI as it is based on IR observations. These external parameters are mainly the height and vertical extent of the dust layer, which influences the $T_{10.8}$ observations to a high degree (Pierangelo et al., 2004) and the size of the dust particles, which mainly contributes to the BTD (Wald et al., 1998; Li et al., 2007). Furthermore both $T_{10.8}$ and BTD are also influenced by the mineralogical composition of the dust (e.g. Ackerman, 1997).

The selected observation times for deriving BMDI bound the main dust mobilisation time between 06:00 and 09:00 UTC and are assumed to represent the time of lowest and highest daily atmospheric dust loads (for the Sahara). Thus not only the thermal night-to-day contrast is taken into account, but also the contrast in column dust load is included in the BMDI.

3.3. The March 2006 dust storm: BMDI observations and sensitivity to dust load, viewing geometry and atmospheric water vapour

The dust storm of 6–11 March 2006 is a very prominent example of a Sahara-wide dust storm with strong dust export onto the Atlantic Ocean. A detailed description of this dust storm is given e.g. in Tulet et al. (2008). The influence of the different included components onto the BMDI together with “dust” scheme RGB images of MSG IR observations has been presented above for March 7. In Fig. 3 the evolution of the dust storm in the Sahara and Arabia domain is shown in terms of BMDI mapped onto a 0.5° × 0.5° grid.

It should be remembered that low BMDI values represent high dust loads. The evolution of the dust front over the Western and Southern Sahara into the Sahel domain and onto the Atlantic Ocean is very good represented by the BMDI values. A clear separation between low and higher BMDI values is evident with BMDI values lower than approximately 5–6 K indicating the presence of airborne dust (see also Tulet et al., 2008).

All BMDI observations of the Period March 6–March 11, 2006 have been compared to MODIS “Deep Blue” AOD observations (MODIS AOD hereafter) with respect to the viewing geometry. Daily MODIS observations were mapped onto the same 0.5° grid as BMDI observations. Observations of the Aqua satellite's MODIS instrument are used here, thus MODIS data are generally from local time afternoon hours. It is assumed that the time delay between BMDI (which is inherent of the bitemporal approach) and MODIS observations does not affect the comparison very much over the Sahara domain (in the Eastern Sahara MODIS observation times are very close to 12:00 UTC). The comparison with respect to 12:00 UTC MSG observation sun zenith angle (SZA) is given in Fig. 4a while b presents the comparison with respect to MSG viewing zenith angle (VZA).

For the angular bins presented in Fig. 4, Spearman rank correlation coefficients and linear fit models have been calculated. The respective correlation coefficients and slopes of the fit model are presented in Table 1. Although deviations between correlation coefficients and between slopes of the fit model occur for both SZA and VZA, no clear dependence of rank correlations of either SZA or VZA can be found. The slope of the linear fit shows a dependence of both SZA and VZA. Due to the land–ocean distribution within MSG FOV and the time of year of the presented dust storm, SZA and VZA are closely connected in this analysis and it cannot clearly be concluded if the effects are more due to the sun elevation or due to the viewing zenith angle. Also from Fig. 4 it is clearly evident, that the relation between dust load (MODIS AOD) and BMDI is non-linear, thus the slope of a linear fit model can be regarded only as a first-order approximation for dependencies. As Spearman rank correlations do not rely on linearity of the relation, the small deviations of the correlation coefficients with the viewing geometry can be regarded as a sign for only minor influence of the geometry onto the dust detection capabilities with BMDI.

Please cite this article as: Klüser, L., & Schepanski, K., Remote sensing of mineral dust over land with MSG infrared channels: A new Bitemporal Mineral Dust Index, *Remote Sensing of Environment* (2009), doi:10.1016/j.rse.2009.04.012

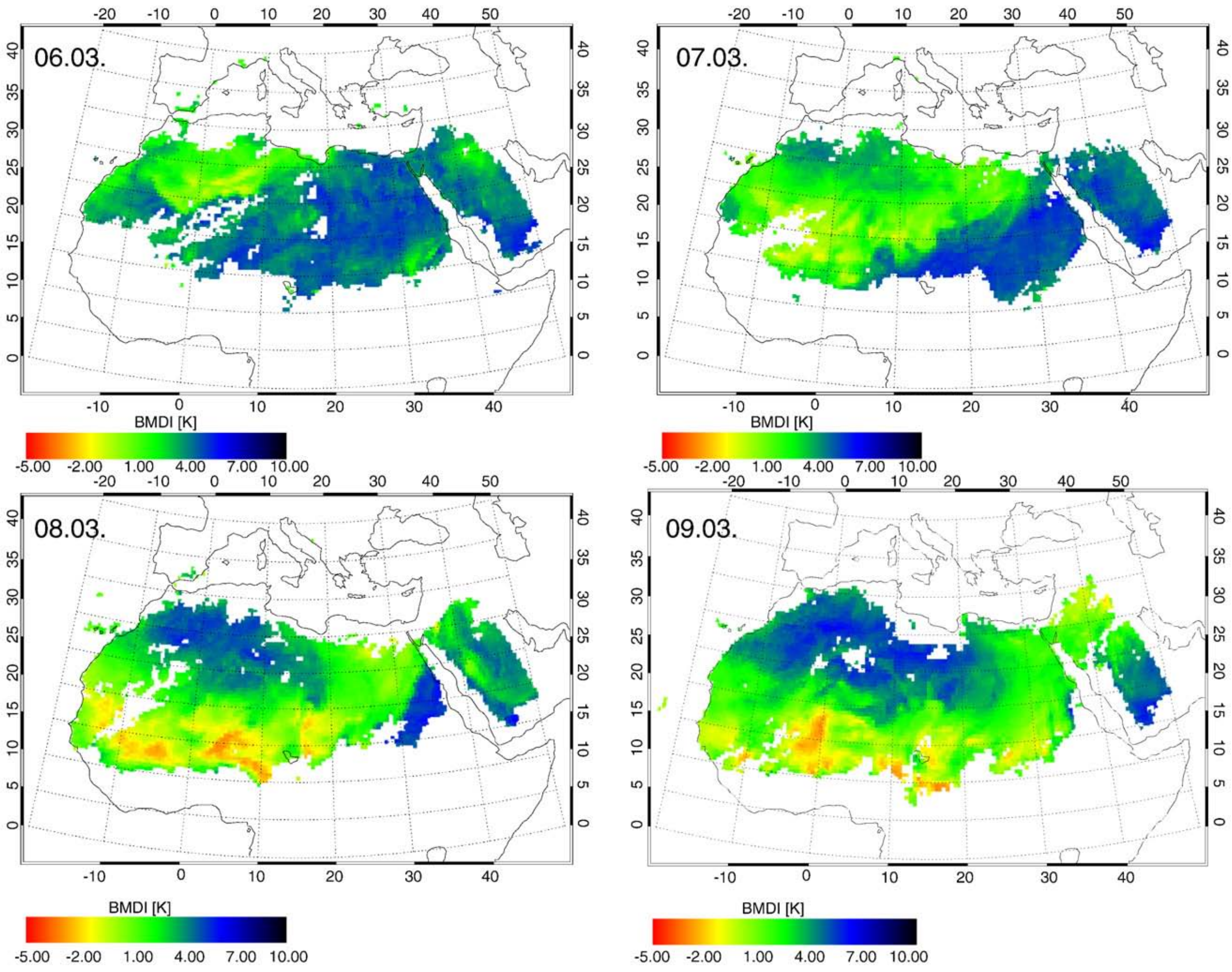

Fig. 3. BMDI maps of the dust storm evolution from March 6–11, 2006 in the Sahara domain. Low BMDI values represent high dust load.

Moreover it follows from Fig. 4, that only BMDI values lower than 6 K occur in the presence of mineral dust indicated also by MODIS. This is consistent with the values found from spatial considerations of the dust front evolution in Fig. 3. On the other hand, also at low AOD values BMDI is derived in some cases. These low BMDI values at low AOD can be explained with the influence of dust layer height onto $\Delta T_{10.8}$ in Eq. (6) and the dust particle size onto BTD (e.g. Li et al., 2007) and thus also onto ΔBTD in the case of moving dust plumes. From these observations it can be concluded that there is no lower bound for dust load in terms of AOD for which BMDI dust detection is possible.

From Fig. 4c it is evident, that BMDI dust detection is limited to scenes with moderate or low atmospheric moisture. For WVC greater than 3 cm dust detection is still possible in some scenes but not reliable. Generally it can be inferred that the WVC influence on BMDI dust detection is pronounced strongest for dust AOD lower than 0.5, while for higher AOD (higher dust load) the BMDI dust detection is more independent from WVC values (below the limit of 3 cm). Furthermore, strong dust events associated with high atmospheric dust loadings and therefore high AOD values are mainly related with low WVCs. The 3 cm dust detection limit corresponds very well with the findings of Legrand et al. (2001) regarding the limitation of infrared dust detection in environments of high atmospheric moisture. Fig. 4d shows all BMDI values (0.5° grid) of the 6–11 March 2006 dust storm compared with corresponding WVC values. No clear evidence of WVC influence on BMDI values is present. The Spearman rank correlation coefficient between BMDI and WVC is $r = -0.291$. The anti-correlation, in contrast to the theoretical increasing influence of atmospheric water vapour on BMDI (see also Section 4.2; low BMDI represents higher dust load), is assumed to be the result of the higher dust loads being transported in very dry air, which is very common for mineral dust in Northern Africa.

4. Evaluation of the Bitemporal Mineral Dust Index (BMDI)

4.1. Spatial distribution of BMDI observations

For statistical analysis and evaluation of dust detection with BMDI, observations have been re-mapped to a 0.5°×0.5° grid covering the MSG FOV for a better comparability with other satellite products. In order to estimate the average annual dust load as determined with BMDI arithmetic mean values, grid boxes for which no BMDI is available are set to the maximum BMDI value (representing minimum dust load).

Using this approach means to assume, that e.g. in the case of clouds no dust is present in the atmosphere. This assumption is obviously incorrect (Miller et al., 2008). Replacing missing values with the maximum BMDI value means that the annually averaged dust load is not substantially overestimated, a problem that would occur if only the values of valid BMDI observations were included in the averaging procedure. Largest errors are estimated for areas of sporadic dust episodes where values of single grid boxes have highest impact on the

Please cite this article as: Klüser, L., & Schepanski, K., Remote sensing of mineral dust over land with MSG infrared channels: A new Bitemporal Mineral Dust Index, *Remote Sensing of Environment* (2009), doi:10.1016/j.rse.2009.04.012

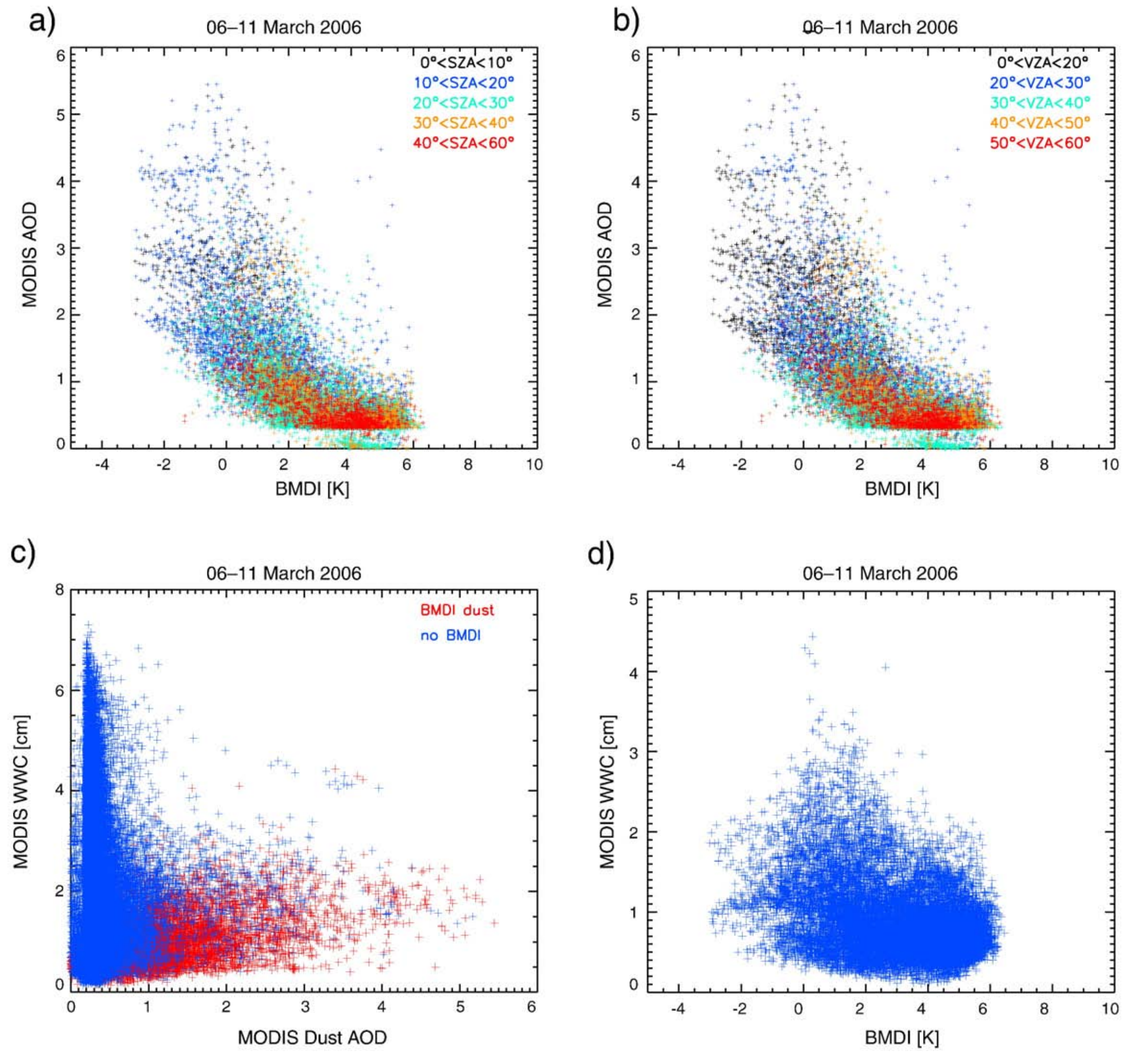

Fig. 4. Comparison of BMDI and MODIS Deep Blue AOD for the March 2006 dust storm in the Sahara domain: Symbol colours represent different sun zenith angle (a) and viewing zenith angle (b) bins. MODIS Water vapour column (WVC) influence on BMDI dust detection (c) and BMDI values (d). SZA and VZA have no large influence on the BMDI values. Furthermore these plots show the non-linear relation between BMDI values and MODIS AOD. Corresponding rank correlations for the respective angle bins are given in Table 1. Dust detection is possible for WVCs up to 3 cm. (For interpretation of the references to colour in this figure legend, the reader is referred to the web version of this article.)

averaged mean. This is especially the case over the Sahelian sector and Southern Europe. Thus annual averages of gridbox BMDI are calculated by

$$\begin{aligned} \overline{\mathrm{BMDI}} &= \sum_{t=1}^{n} \mathrm{BMDI}(t) \\ \mathrm{BMDI}(t) &= \begin{cases} 10\,\mathrm{K}, & \text{BMDI not derived} \\ \mathrm{BMDI}, & \text{BMDI derived} \end{cases} \end{aligned} \tag{7}$$

in order to derive spatial patterns of BMDI dust load.

Fig. 5a shows the average BMDI values as calculated by Eq. (7) for January–December 2006 on a 0.5°×0.5°-grid together with the temporal variance of the gridbox BMDI (Fig. 5b). Over source regions like the Bodélé Depression and the Western Sahara, low average BMDI values occur, representing high average dust load. Also areas of elevated terrain such as the Aïr Mountains, the Atlas Mountains or the Hoggar Mountain ridge are represented in mean BMDI as high values (low dust load), building up pathways for dust transport in between. BMDI variance is high in the southern part of the Sahara domain, where episodic dust export to the south is the predominant feature of atmospheric dust load.

4.2. Comparison with AERONET AOD

Observations from AERONET (Holben et al., 1998) level 2 data have been used to determine the possibility and accuracy of detecting mineral dust with the BMDI. One year (2006) of aerosol observations is used to evaluate the BMDI.

Table 2 lists the eight AERONET stations with a reasonable length of observation periods during 2006 as well as the number of days, for which AOD observations are available. These stations compose a total

Table 1
Rank correlation coefficients and respective linear fit slopes for the 6–11 March 2006 dust storm in the Sahara and Arabia domain in dependence of the sun zenith and viewing zenith angles.

		0°–10°	10°–20°	20°–30°	30°–40°	40°–60°
SZA	Correlation	−0.532	−0.754	−0.645	−0.641	−0.663
	Fit-slope	−0.349 K^{-1}	−0.305 K^{-1}	−0.186 K^{-1}	−0.201 K^{-1}	−0.185 K^{-1}
VZA	Correlation	−0.583	−0.732	−0.573	−0.656	−0.667
	Fit-slope	−0.324 K^{-1}	−0.288 K^{-1}	−0.146 K^{-1}	−0.201 K^{-1}	−0.185 K^{-1}

Between angles and correlation coefficients no clear relation is evident while the slopes of the linear fit (which is not the best fit model, as can be easily seen in Fig. 4) seem to depend on the viewing and sun zenith angles to some degree.

Please cite this article as: Klüser, L., & Schepanski, K., Remote sensing of mineral dust over land with MSG infrared channels: A new Bitemporal Mineral Dust Index, *Remote Sensing of Environment* (2009), doi:10.1016/j.rse.2009.04.012

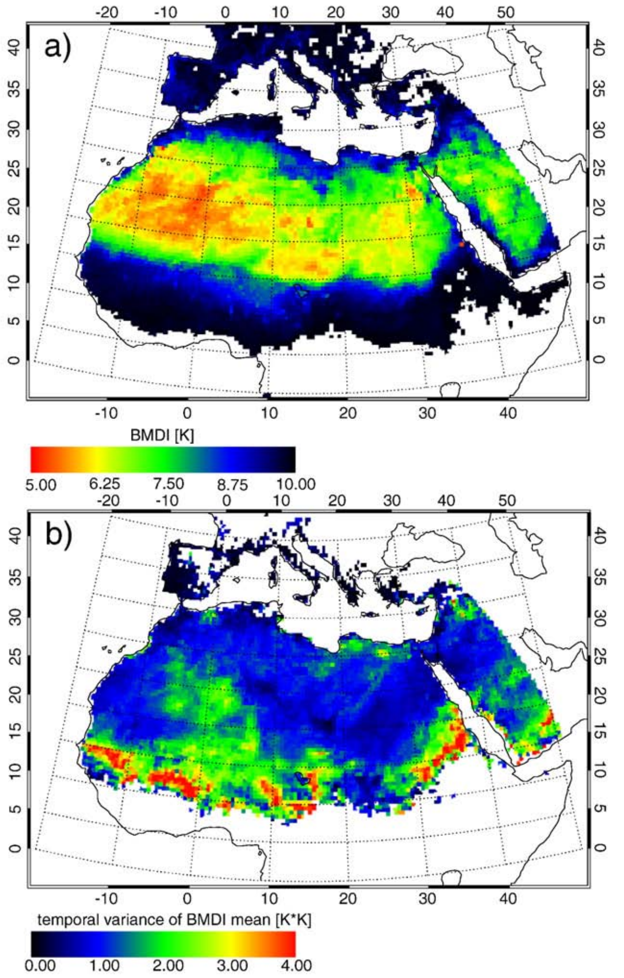

Fig. 5. Mean gridbox BMDI as obtained from Eq. (7) (a) and temporal variance of gridbox BMDI for 2006 (b). For contrast enhancement the colour bar in (a) is bound to [+5 K, +10 K], lower BMDI values represent higher dust loads. (For interpretation of the references to colour in this figure legend, the reader is referred to the web version of this article.)

of 1939 AOD observation days used for comparison with the BMDI. AERONET provides AOD at different wavelengths, from which the Ångström exponent α can be derived by the following equation:

$$\frac{AOD_{0.44}}{AOD_{0.87}} = \left(\frac{0.87\,\mu\text{m}}{0.44\,\mu\text{m}}\right)^{\alpha} \tag{8}$$

The Ångström exponent is often used to estimate aerosol size information (e.g. Dubovik et al., 2002).

Aerosol plumes located around the Sahara may often consist of more than one aerosol layer, typically a layer of biomass burning aerosol over- or underlying a desert dust aerosol layer (see e.g. McConnell et al., 2008 for details). This takes place most often during the Sahelian dry season (October–May), which also is the season of most southward desert dust transport (Engelstaedter et al., 2006; Engelstaedter & Washington, 2007; Schepanski et al., 2009). Thus one should bear in mind that AERONET AOD represents the combined extinction of biomass burning aerosol and mineral dust (Hsu et al., 2004; McConnell et al., 2008).

Table 2
List of AERONET stations used together with their geographical positions, station heights above sea level (a.s.l.) and numbers of days with available AOD observations.

Station	Geogr. position	Height a.s.l.	Observation days
Agoufou	15.34°N/1.48°W	305 m	258
Banizoumbou	13.54°N/2.67°E	250 m	286
Dakar	14.48°N/16.96°W	0 m	283
Djougou	9.76°N/1.59°E	400 m	245
DMN Maine Soroa	13.22°N/12.02°E	350 m	222
IER Cinzana	13.28°N/5.93°W	285 m	250
Niamey	13.48°N/2.17°E	205 m	112
Solar Village	24.91°N/46.40°E	764 m	283

In Fig. 6a the comparison of AERONET AOD observations and BMDI observations for 3×3 MSG pixel box (9 km×9 km at nadir) averages centered at the AERONET station site is shown. As it is assumed, that the BMDI is most strongly influenced by the dust load at daytime observations (12:00 UTC) and no sunphotometer observations are possible during nighttime, AERONET observations are averaged over the time interval 11:00–12:00 UTC for the comparison. The error bars in Fig. 6a represent AERONET standard deviations over this one-hour interval.

AERONET observations are filtered by the dust criterion

$$\begin{aligned} AOD_{1.020} &\geq 0.1 \\ \alpha &< 0.6 \end{aligned} \tag{9}$$

adapted from Dubovik et al. (2002) and in a slightly different form also used by Schepanski et al. (2007). Although these conditions

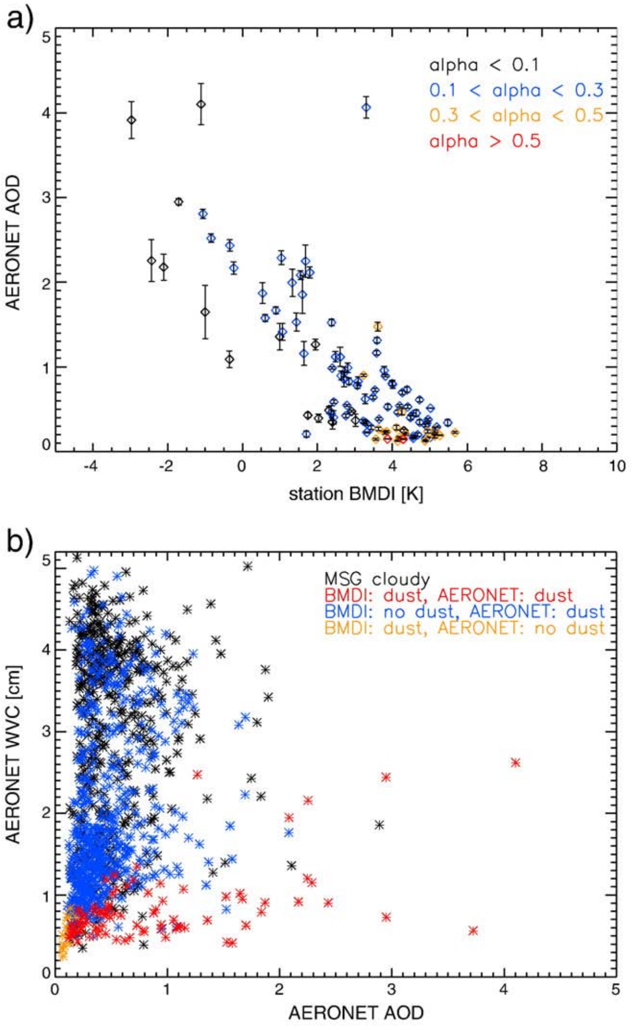

Fig. 6. Scatter plot of BMDI observations and AERONET AOD for eight selected AERONET stations (Table 2) divided into Ångström exponent classes of $\alpha<0.1$, $0.1<\alpha<0.3$, $0.3<\alpha<0.5$ and $\alpha>0.5$ (a) and comparison of AERONET AOD and AERONET water vapour column (WVC) with BMDI dust detection (b). Erros bars in (a) are standard deviations for the one-hour averaging interval of the AERONET observations. Low BMDI values represent high dust loads. (For interpretation of the references to colour in this figure legend, the reader is referred to the web version of this article.)

Please cite this article as: Klüser, L., & Schepanski, K., Remote sensing of mineral dust over land with MSG infrared channels: A new Bitemporal Mineral Dust Index, *Remote Sensing of Environment* (2009), doi:10.1016/j.rse.2009.04.012

exclude AOD observations originating from non-dust aerosols, a contribution of possible biomass burning aerosols to AOD in dusty scenes is not excluded (Table 3).

After dust filtering of the AERONET observations, a total of 162 observations of both BMDI dust and AERONET dust, remains.

In Fig. 6a symbol colours represent Ångström exponent classes. As expected, BMDI is anti-correlated with AOD and shows a linear correlation coefficient of $r = -0.796$. Again, BMDI values are well below 6 K for all AERONET dust observations and BMDI is also derived for low AOD values in some scenes (compare the results in Section 3.3).

Observations with high AERONET AOD and large deviations from an assumed fit curve range also show large standard deviation in the AERONET observations over the one-hour averaging interval. These events are very likely to represent days with high variability of atmospheric dust load, which strongly affects the BMDI due to its bitemporal character.

AERONET observations use the solar spectral range and the BMDI is derived from thermal infrared observations. Both observations depend on dust particle size, but in different regions of the size spectrum. Pierangelo et al. (2004) give an overview of problems with comparison of solar and IR dust observations. The BMDI is mainly determined by coarse and very large dust particles (see e.g. Brooks & Legrand, 2006), while AERONET AOD is also a result of the fine mode aerosol fraction. AERONET AOD also includes biomass burning aerosol contributions to which the BMDI value is insensitive. From an analysis of Pierangelo et al. (2004) and the discussion in Section 3 it follows, that also the BMDI is dependent not only on aerosol load and aerosol particle size, but also on dust layer height due to the inclusion of $\Delta T_{10.8}$. Thus a strictly linear behaviour cannot be expected between BMDI and AOD. Especially for large α (orange and red symbols in Fig. 6a), low BMDI values occur at very small AERONET AOD. Those α values indicate quite small particle sizes, which often occur in aged dust layers transported in cold air above the BL. Following the findings of Pierangelo et al. (2004), for those scenes the low BMDI values are assumed to be the result of a high dust layer altitude at an overall low solar AOD, reflecting the height dependency of the BMDI.

Fig. 6b shows AERONET AOD observations compared to water vapour column (WVC) values as retrieved from AERONET. It is highly evident, that BMDI dust detection is only possible for low humidity values or in some cases for moderate humidity in combination with very high dust load. On the other hand, most cases with failed BMDI dust detection despite cloud-free conditions take place in scenes with moderate dust loads and high WVC observations. Generally from Fig. 6b can be concluded, that dust detection with the BMDI is only possible at WVC lower than approximately 2.5 cm. For moderate and low AOD (<0.5) this value decreases to about 1.0 cm. Thus dust detection with BMDI is limited to dry air environments as they are present e.g. in the central Sahara or also in dry air outbreaks into the Sahel domain along the ITD.

4.3. Dust detection compared to MODIS AOD and OMI AI

From MODIS observations AOD can be retrieved also over bright land surfaces with the "Deep Blue" algorithm (Hsu et al., 2004). In this analysis MODIS observations from the Aqua satellite have been used (available online at *http://ladsweb.nascom.nasa.gov*). "Deep Blue" 0.55 µm AOD (referred to as MODIS AOD) is also sensitive to different types of aerosol including fine mode particles such as soot from biomass burning (see Hsu et al., 2004 for details).

The "Deep Blue" retrieval is assumed to be nearly insensitive to aerosol layer height (Hsu et al., 2004).

Daily MODIS AOD is mapped onto a 0.5°×0.5° grid for analysis, as it is done for BMDI observations. Only AOD values larger than 0.2 (representing significant dust load) and with Ångström exponents below 0.6 (equivalent to the AERONET dust filtering in Eq. (9)) are taken into account, as they are assumed to show mainly mineral dust or at least pixels having significant dust contributions (adapted from Dubovik et al., 2002). Dust presence can be obtained from BMDI observations by an threshold of 6 K, which results from the analyses presented above (AERONET comparison and the March 2006 dust storm).

Although it is not very likely as indicated by the above results, this dust detection threshold can lead to a slight underestimation of dust activity for events with low dust loads. But the same is true for all thresholds applied to AOD observations as presented below. Fig. 7a shows the number of days with dust activity in 2006 as observed with BMDI. MODIS "Deep Blue" dust observation numbers for 2006, indicated by the dust filtering described above, are shown in Fig. 7b while c shows the number of aerosol observations with OMI AI (AI>1). The AI does not distinguish between mineral dust and biomass burning aerosol or classify mixed aerosol layers. Thus Fig. 7c incorporates also biomass burning aerosol plumes, which are assumed to contribute to AI over the Guinea coast region and the Sahel sector to a very high degree.

White areas are gridboxes with no observations of the respective algorithm at all. One should remember that only "Deep Blue" AOD having passed the dust filtering described above is incorporated here for MODIS. The spatial patterns of numbers of dust observation in Fig. 7a–c all present frequent dust presence in the Western Sahara and the Bodélé Depression region. Also areas of elevated terrain are evident in all three observation data. The spatial differences of the frequency of dust presence as seen from those three observation methods are affected by several aspects. All three considered dust detection methods show different sensitivities to dust layer height, negligible in the case of MODIS AOD, while BMDI and OMI AI are height dependent. Also the particle size spectrum influences the number of observations. The BMDI is sensitive to large particles only, while MODIS AOD and OMI AI also are sensitive to fine mode particles and mixed aerosol species. Thus in cases of airborne dust with low concentrations of large particles, those dust plumes are more likely to be detected by MODIS or OMI than by BMDI, while in cases with a higher fraction of large particles at overall low AOD, plumes are more likely to be detected by BMDI than by the other methods. Furthermore, the dust filtering of the MODIS observations might also reduce the number of dust observations by means of MODIS AOD. Especially the AOD threshold of 0.2 might exclude some thin and high aged dust layers indicated by low BMDI values, which is also evident in the AERONET analysis (Fig. 6a). Those thin dust layers mostly occurs over regions, which are not primarily active dust source areas. Fig. 7d shows the difference in dust detection numbers between MODIS and BMDI. It is evident that numbers of dust observation are lower for MODIS than for BMDI between strong dust source areas (see also Schepanski et al., 2007), where thin layers of transported dust can be assumed to be a significant contribution to the BMDI, while not being detected by the MODIS observations with the filtering method used here. In areas with regular influence of moist air such as coastal areas around the Sahara and in the Sahel domain where moist air is predominant south of the ITD, BMDI dust observation times are much lower than those of MODIS, again showing the limitation of IR dust detection in environments of high humidity (see also Section 4.5).

Table 3
AERONET and MSG dust observation numbers for the selected AERONET stations.

Total AERONET observations	1939
AERONET observations after dust filtering	1299
MSG cloudy/AERONET observations	452
BMDI dust/AERONET dust	162
BMDI no dust/AERONET dust	685
BMDI dust/AERONET no dust	32
BMDI no dust/AERONET no dust	108

As can be seen from Fig. 6b, the large number of AERONET dust detections with no BMDI detection results mainly from the influence of atmospheric water vapour on the BMDI dust detection at moderate dust loads. Numbers of AERONET observations showing aerosol different from mineral dust are also given for comparison.

Please cite this article as: Klüser, L., & Schepanski, K., Remote sensing of mineral dust over land with MSG infrared channels: A new Bitemporal Mineral Dust Index, *Remote Sensing of Environment* (2009), doi:10.1016/j.rse.2009.04.012

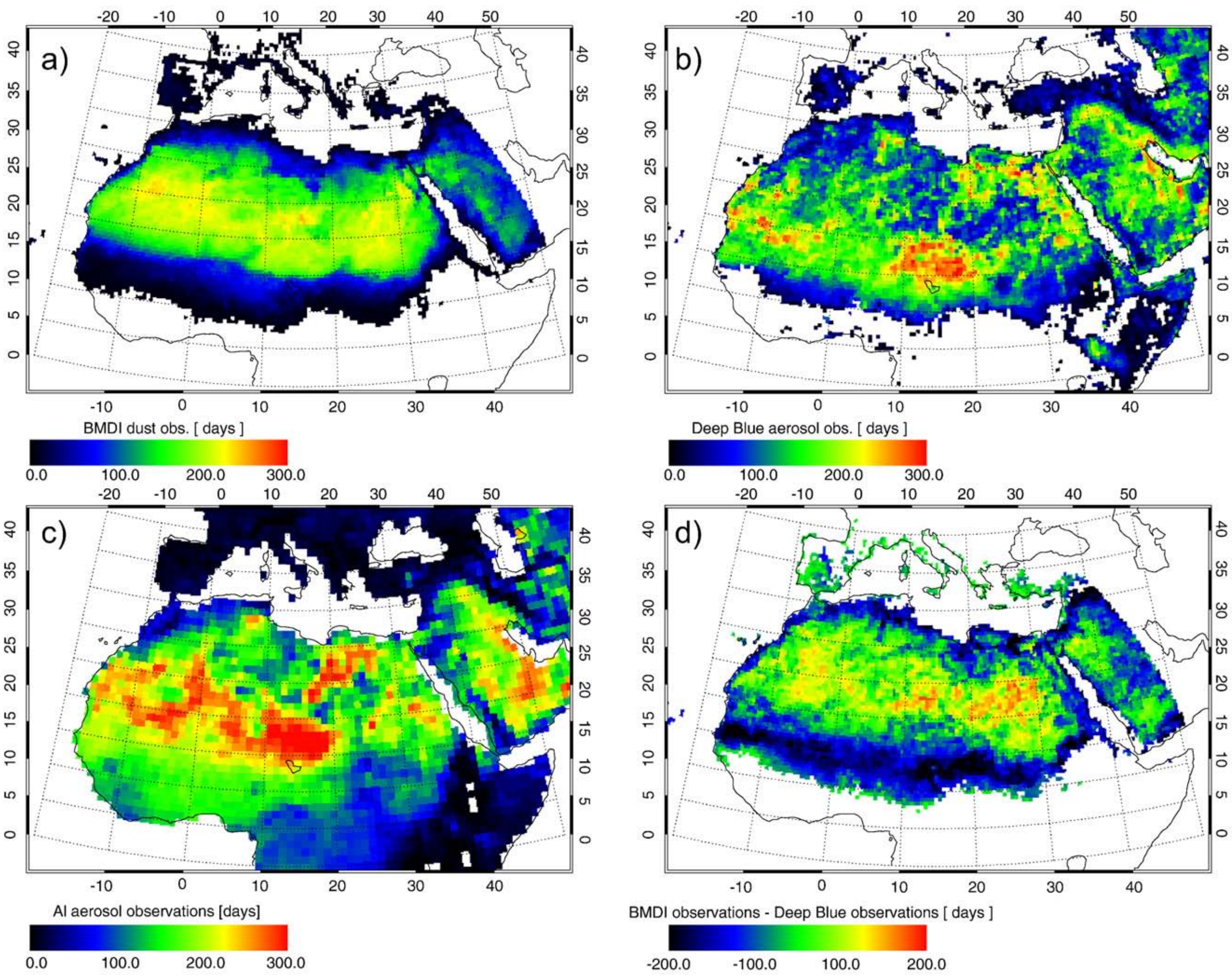

Fig. 7. Number of days with dust detected in 2006 by BMDI (a), by MODIS AOD (b), and by OMI AI (c). In (d) the difference between BMDI observation numbers and MODIS Deep Blue observation numbers is shown.

Furthermore, the BMDI represents the airborne dust as a difference between noon (12:00 UTC) and the previous night (03:00 UTC), while MODIS and OMI acquire single-time dust observations.

Also the role of different cloud screening techniques in the MODIS and OMI products and BMDI, the positions of clouds to the different observation times and orbital parameters of the different satellites remains unclear with respect to their contribution to the numbers of dust observations.

4.4. Correlation analysis

Fig. 8 presents gridbox correlations between BMDI and MODIS AOD (Fig. 8a) and between BMDI and OMI AI (Fig. 8b). Correlation coefficients are calculated as Spearman rank correlations (Spearman, 1908). Gridboxes with less than five days of common MODIS and BMDI aerosol observations are treated as missing data.

Magnitudes of anti-correlation are quite high in the areas of high numbers of dust observations and high mean dust loads (see Fig. 7) and partly in the South-Sahara domain, while along mountain sides such as the Atlas, the Aïr and the Red Sea Mountains (see Fig. 8c) rank correlations between BMDI and AOD are very small in magnitude. In elevated complex terrain with eventually steeper slopes (e.g. on the Sinai Peninsula and the Red Sea Mountains) correlations even become positive, which is thought to be an effect partly of viewing angle and partly of terrain height (which also contributes to BMDI and AOD values).

Very high magnitudes of anti-correlation between BMDI and MODIS AOD also occur around the Akhdar Mountains. This region in northern Libya at the east coast of the Gulf of Sidra is frequently affected by cyclones (Alpert & Ziv, 1989) in spring and early summer.

Fig. 8b shows rank correlation coefficients between BMDI and OMI AI. As in the case of the comparison with MODIS AOD, the AI correlations are also mainly negative, and inhibit in some regions quite large magnitudes, especially over the main source regions and along the southern boundary of the Sahara.

The spatial patterns look very similar, although in some regions magnitudes of anti-correlation are significantly smaller than it is the case for MODIS. This may be partly due to the coarser resolution of the OMI AI data and partly due to the different height dependencies of BMDI and OMI AI.

For scenes with low correlation it needs to be kept in mind that the local BMDI values depend on atmospheric column dust load as well as on surface temperature due to the use of $T_{10.8}$. Surface temperatures are already lower in elevated terrain compared to possible surface temperatures at sea level, a fact that impacts on the BMDI values. Also mountain shadows affect not only surface temperatures along the mountain slopes, but also AOD retrievals as for mountain slopes insolation and sun zenith angle differ strongly from values over flat terrain. Consequently, the interpretation of correlation analysis for satellite based aerosol observations in mountainous terrain is a very difficult task. Nevertheless, over the major Saharan source areas as the Bodélé Depression, Western Sahara and the foothills of the Aïr

Please cite this article as: Klüser, L., & Schepanski, K., Remote sensing of mineral dust over land with MSG infrared channels: A new Bitemporal Mineral Dust Index, *Remote Sensing of Environment* (2009), doi:10.1016/j.rse.2009.04.012

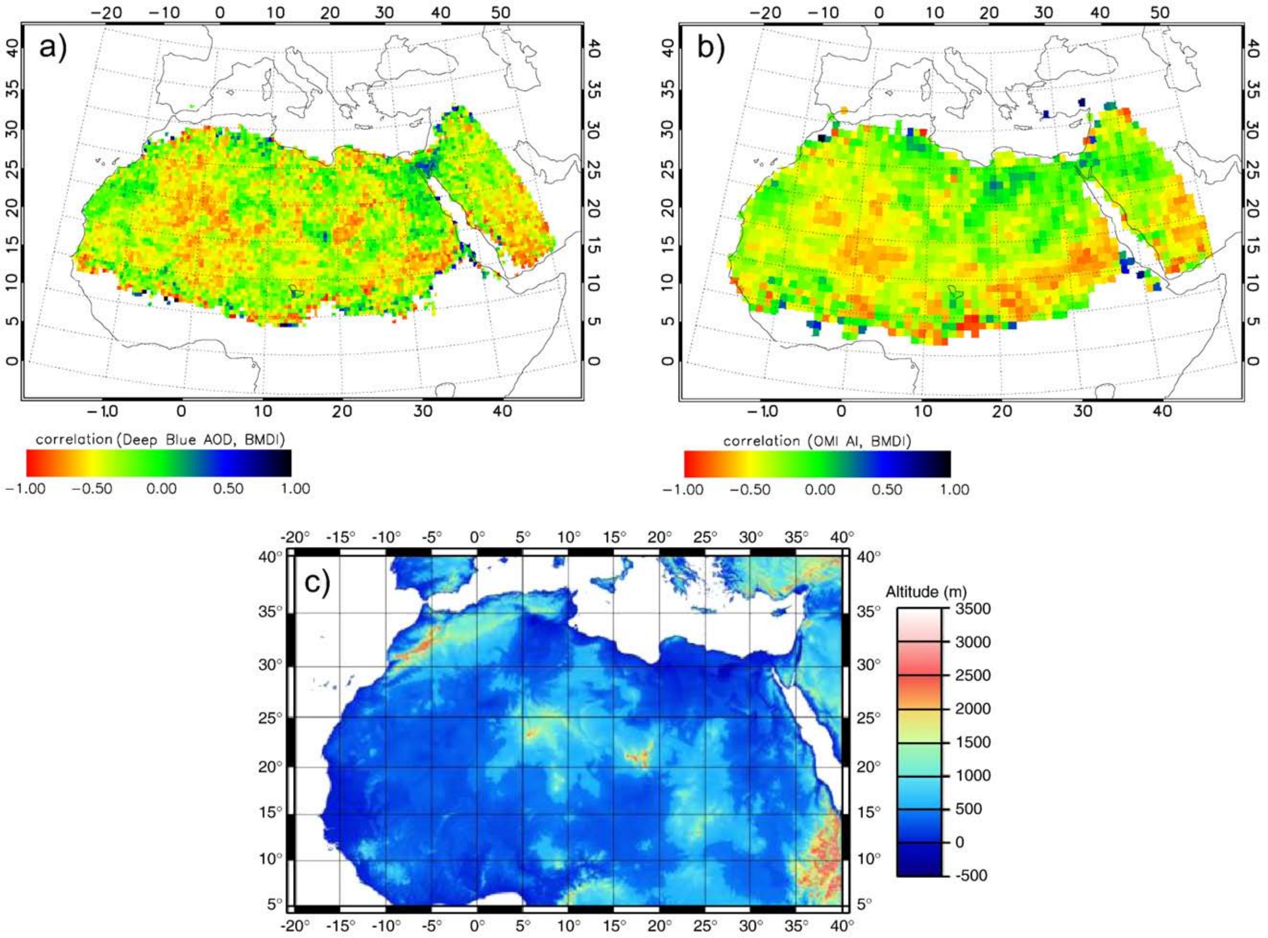

Fig. 8. Spearman rank correlations between BMDI and MODIS AOD (a) and between BMDI and OMI AI (b) for 2006 and a map of the topography of the Sahara for comparison (c). Topography is taken from the digital elevation data set GTOPO30 provided by the U.S. Geological Survey.

Mountains, correlations are high in magnitude and show good results in dust detection with BMDI.

4.5. Comparison of BMDI dust detection with MODIS WVC

In Fig. 9 seasonal BMDI observations are compared with Water Vapour Column retrieved from MODIS observations. After application of Eq. (7) to the BMDI observations Spearman rank correlations between BMDI values and MODIS WVC (for gridboxes with at least 5 BMDI observations per period) have been calculated. They are shown for October–April in Fig. 9a and for May–September in Fig. 9b. The seasonal cycle of WVC is presented in Fig. 9c and d, showing the mean WVC for October–April (sub-Saharan dry season) and May–September (sub-Saharan monsoon season), respectively.

Water vapour columns of more than 3 cm (limit for BMDI dust detection) are quite common in the monsoon season of sub-Saharan Africa, but are quite rare during the dry season being the season with main dust activity in this region. Over most parts of the Sahara correlation magnitudes are small, showing no clear relationship between BMDI and WVC. But there are also regions with higher magnitudes of positive correlations (indicating higher BMDI values representing lower dust load in scenes with high WVC). The patterns of higher correlation magnitudes differ between the seasons. During the dry season correlations are highest in the sub-Saharan Sahel region. This corresponds to the results of Fig. 7d, where MODIS dust observation numbers were much higher in the sub-Saharan Sahel than those of BMDI. One explanation for the high correlation magnitudes between BMDI and WVC is that the dust transport towards the Sahel takes place within very dry air (harmattan winds) while moist air outbreaks towards the north are mostly connected to very low dust activity in that region. In the region of the Bodélé Depression and the Tibesti mountain ridge correlation magnitudes are very low during the dry season, which is the season of main dust emission from the Bodélé (see also next section). Here the correlation between BMDI and WVC increases significantly during the sub-Saharan monsoon season (May–September), where Bodélé dust activity decreases and moist air intrusion to the area is quite common (Fig. 9d). Correlation magnitudes of the Western Sahara region including the Aïr mountains dust source region are very low during May–September (Fig. 9b), the main season for Western Sahara dust emission. Also here monsoonal moist air intrusion is quite common (Fig. 9d), but the negative correlations between BMDI and WVC (low BMDI together with high WVC) occurring in the area indicate, that also during such events of increased atmospheric humidity BMDI is capable of dust detection in the region. From the differences in seasonal correlation patterns between BMDI and WVC it is evident that BMDI mainly reflects the emission activity of the different Saharan dust source areas. The seasonal cycle of atmospheric water vapour, while clearly affecting BMDI as shown above, is not the predominant feature in BMDI dust detection.

5. Time series of dust load as seen from BMDI observations

Not only spatial patterns of airborne dust can be inferred from BMDI observations, but also the temporal evolution of mineral dust load in restricted areas.

Please cite this article as: Klüser, L., & Schepanski, K., Remote sensing of mineral dust over land with MSG infrared channels: A new Bitemporal Mineral Dust Index, *Remote Sensing of Environment* (2009), doi:10.1016/j.rse.2009.04.012

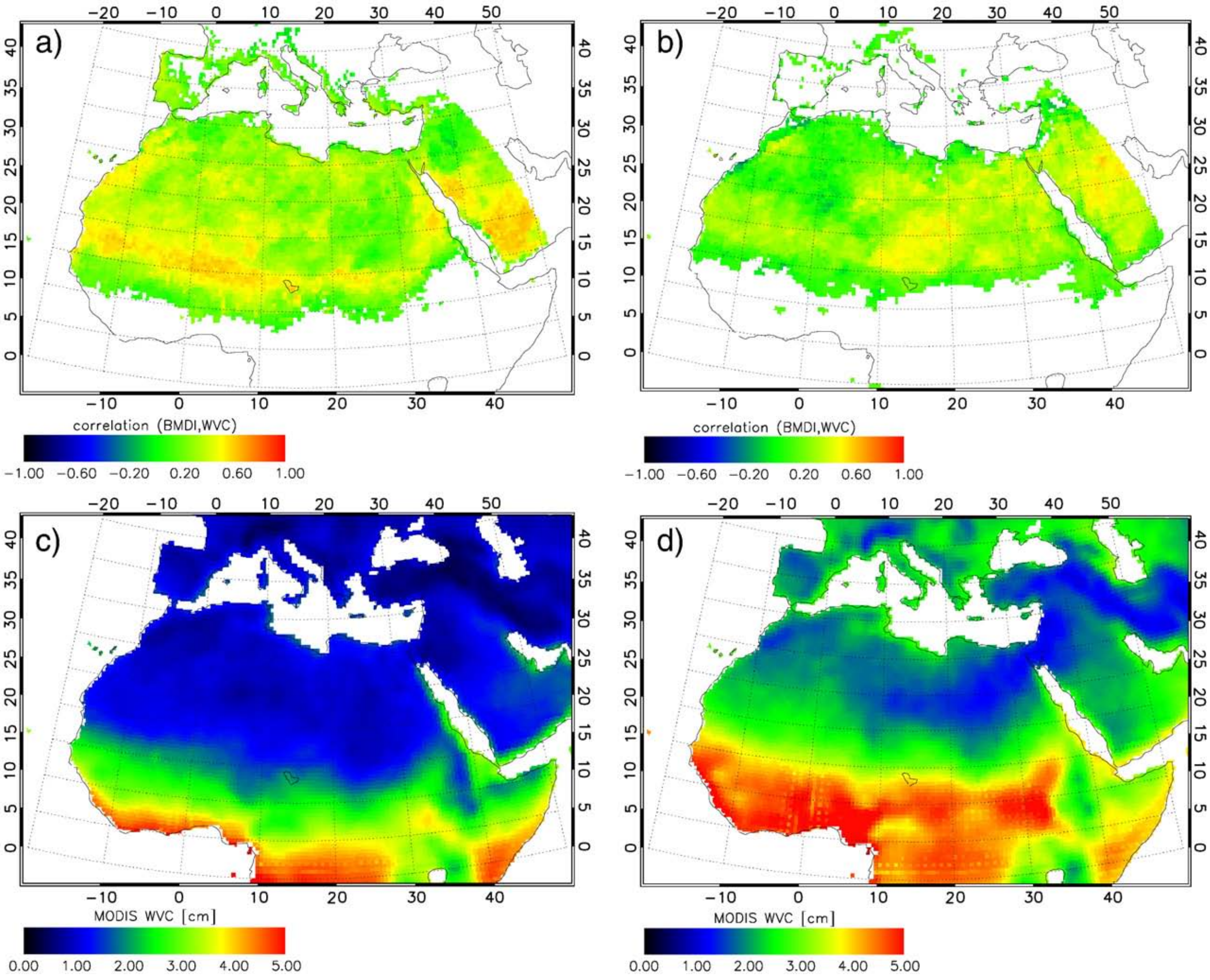

Fig. 9. Spearman rank correlations between BMDI and MODIS WVC for Oct–Apr (a) and for May–Sep (b) together with mean WVC (c and d, respectively).

Fig. 10 shows the pre-defined sub-regions as red boxes which are supposed to represent important dust source areas in northern Africa. Land surfaces are shaded with mean Normalised Difference Vegetation Index (NDVI) values of 2006 (Richard et al., 2008). Low NDVI indicates no vegetation while high NDVI shows high vegetation fraction.

Those pre-defined regions are the Aïr mountains region (AI), the Akhdar desert region (AK), the Bodélé Depression (BO), the Western Sahara (WS).

Fig. 11 shows BMDI time series for the year 2006 of four source regions together with the area-averaged cloud cover at 12:00 UTC as detected by APOLLO. Area mean BMDI values were calculated with Eq. (7) for days with dust observations present in the area. Thus gridboxes without BMDI observations are included with BMDI of 10 K in order to include the same number of observations daily. Every day all grid boxes within the pre-defined restricted sub-region are averaged for analysis.

One of the source regions for summer dust export to the Atlantic is the region around the Aïr, Adrar and Hoggar Mountains (Prospero et al., 2002; Schepanski et al., 2009), referred to as Aïr region (AI in Fig. 10).

The time series for this source region for BMDI values, MODIS AOD and cloud cover are given in Fig. 11a. The blue curve indicates area mean BMDI values while the red curve represents area mean MODIS AOD. The area cloud cover is shown by the orange curve. Clouds are not a very common phenomenon in this region, only some episodes of increased cloudiness are evident. In the beginning of the year low BMDI values are evident, indicating high dust loads as often reported in the literature. Also in spring, dust is a prominent feature in the region, often being of strong episodic nature.

During May dust load is reduced to some extent. After another strong dust episode in June, BMDI values rise, indicating low dust

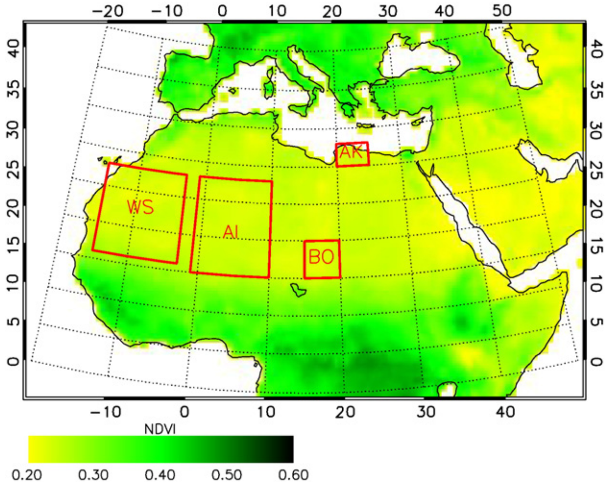

Fig. 10. Dust source areas for area-averaged time series analysis, land cover background is mean NDVI as obtained from MSG observations for 2006. (For interpretation of the references to colour in this figure legend, the reader is referred to the web version of this article.)

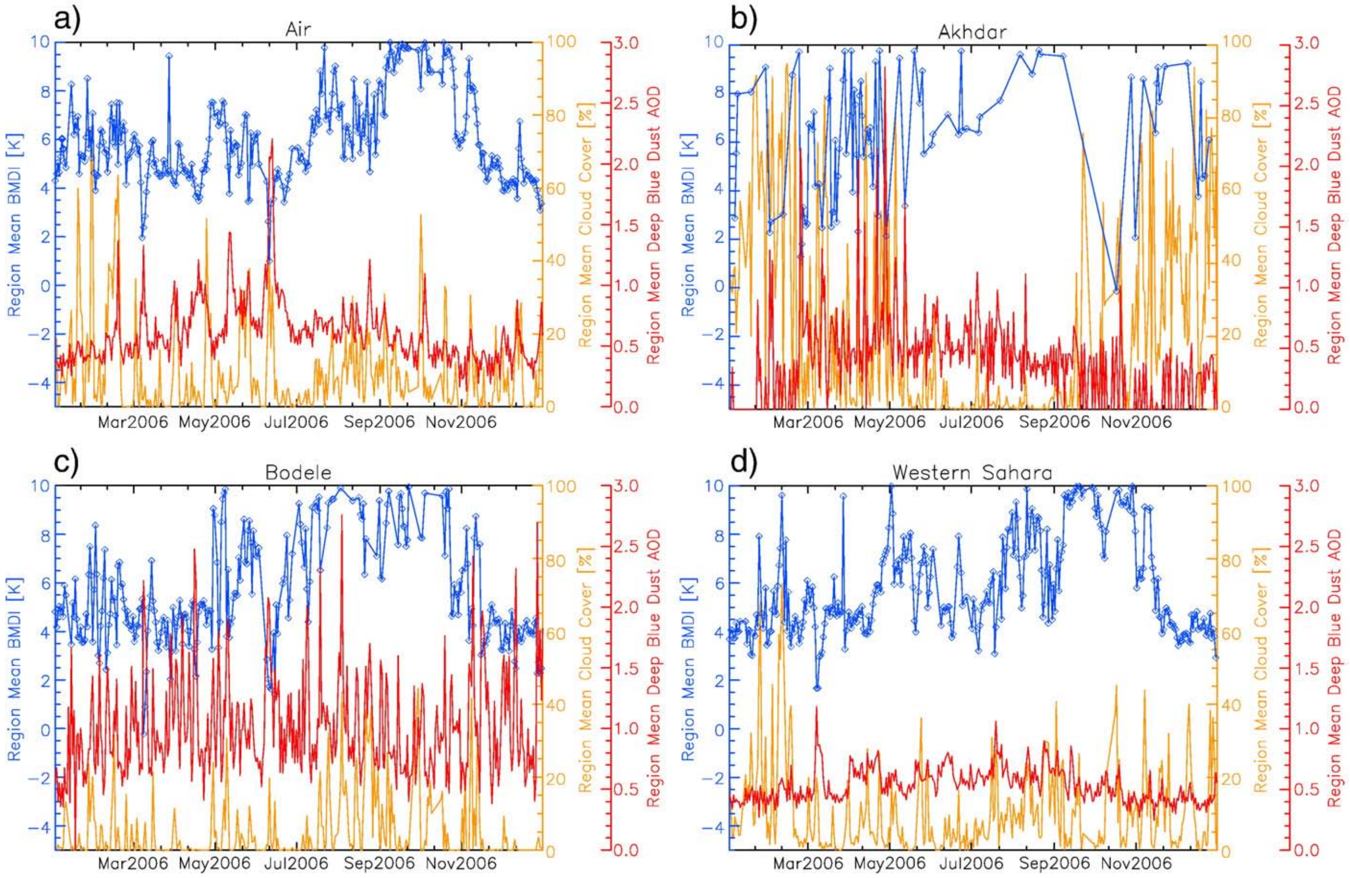

Fig. 11. Area-averaged BMDI (blue), MODIS AOD (red) and cloud cover (orange) time series for the dust source regions Aïr (a), Akhdar (b), Bodélé (c) and Western Sahara (d) in 2006. Low BMDI represents high dust load. (For interpretation of the references to colour in this figure legend, the reader is referred to the web version of this article.)

activity, interrupted by moderate low BMDI values in August and September. After a period of nearly dust-free conditions in autumn BMDI values again decrease and indicate the beginning of a new cycle of winter dust activation. This seasonal cycle and its episodic character are also found in the MODIS observation, where highest AOD is present in May–June. This could be the result of the height dependence of BMDI and the change in dust transportation height over the course of the year.

The Akhdar region (AK, Fig. 11b) is also an active dust source region (Schepanski et al., in press), which becomes evident in the high correlation magnitudes between BMDI and MODIS AOD (see Fig. 8). Although annual dust activity is not so high (Fig. 7, Schepanski et al., in press), this region is of interest for dust transport towards the Mediterranean Sea and Europe. Fig. 5 reveals that the temporal variance of BMDI over this area is as high as e.g. between Aïr and Adrar Mountains (both included in the Aïr time series). This high temporal variance is also indicative for a strong episodic nature of dust load in the region, as can be seen in Fig. 11b. The role of passing cyclones for dust source activation in the Akhdar region can be inferred from the BMDI time series: BMDI values show strong dust episodes during spring, early summer and winter, the seasons of increased cyclonic activity in the Mediterranean region (Pedgley, 1972; Trigo et al., 2002). This is also supported by MODIS observations and the large variance of regional cloud cover during these times. In summer, low dust load is indicated by the BMDI together with very low cloud cover. This can be explained by lower dust source activity as well as by the fact that high dust loads often coincide with high cloud cover fractions due to cyclonic activity.

The Bodélé Depression (BO, Fig. 11c) has been reported to be a very strong dust source region (Prospero et al., 2002; Koren et al., 2006; Schepanski et al., 2007; Schepanski et al., in press).

Fig. 5 marks the Bodélé as one of the regions with very low mean BMDI values. At the same time a very high temporal variance of BMDI is evident, again indicating the strong episodic nature of dust mobilisation. Additionally, the Bodélé dust sources are most active during the early morning hours, which can be explained by the breakdown of the nocturnal low-level jet (Washington et al., 2006; Schepanski et al., in press; Todd et al., 2008). The BMDI takes into account the noon-time MSG slot, a time when dust is already transported off the early morning source area and the local dust load is reduced by this transport component. Apart from this episodic character of Bodélé dust load, BMDI reveals an annual cycle with dust mobilisation minimum in summer and high dust loads during winter and spring, as reported e.g. by Washington and Todd (2005) and Schepanski et al. (in press). This well reported seasonal cycle is not very strong pronounced in the MODIS observations within the Bodélé region.

Another important source region for mineral dust is the Western Sahara region (WS, Fig. 11d), especially for the dust transport towards the North Atlantic during the summer months. This region is characterised in Fig. 7a as one of the areas indicating lowest annual mean BMDI values beside the Aïr domain. The overall annual cycle is quite similar to that of the Aïr region. Dust observed in the WS region is assumed to be not only dust mobilised here, but also having contributions of dust mobilised further east and being transported westward towards the Atlantic Ocean. The “autumnal dust gap” of WS dust load is interrupted by an episode of increased dust load in

Please cite this article as: Klüser, L., & Schepanski, K., Remote sensing of mineral dust over land with MSG infrared channels: A new Bitemporal Mineral Dust Index, *Remote Sensing of Environment* (2009), doi:10.1016/j.rse.2009.04.012

October, which is not clearly evident in Aïr BMDI. Both MODIS and BMDI observations include well defined seasonal cycles but they seem to be somewhat out of phase with highest MODIS AOD in boreal summer and lowest BMDI in December–February. Although agreement between MODIS and BMDI is good in this region in the analysis of Section 4.3, there is an obvious mismatch in the seasonal cycles of Fig. 11d. One possible reason is the dependence of BMDI on dust transportation heights, which modulates the BMDI towards lower values (equals higher dust loads) in boreal winter than during summer. Another effect possibly increasing BMDI values during the monsoon season is the influence of high water vapour amounts due to the monsoonal flow especially in the Southern part of the region. As is evident from Fig. 9d, WVC reaches high values of 3 cm in average in the Southern part of region WS during the monsoon season, influencing the region averaged BMDI values of the time series in Fig. 11d.

Thus it can be assumed that BMDI values originating from the northern part (dry, Saharan air mass) of the WS region dominate the regional mean shown in Fig. 11d. However, the moisture gradient over the WS area due to the partly present transient from Saharan air mass to monsoonal air mass leads to an inherent weighting of the BMDI values due to their WVC dependence. Episodes of strong dust activity, such as the March 2006 dust storm are temporarily well matched in both time series as strong dust events are mainly associated with low WVC values.

6. Summary and conclusions

The newly developed Bitemporal Mineral Dust Index (BMDI) applied to MSG IR observations over land is used to detect mineral dust.

This new dust index is appropriated to the automatic daily detection of airborne mineral dust and is independent from assumptions concerning atmospheric background aerosol concentrations and surface characteristics. Due to the usage of MSG IR observations the algorithm is able to infer semi-quantitative information on atmospheric dust content over bright surfaces as the Sahara desert. Low computation time and MSG data availability since 2004 allow for statistical analysis of mineral dust transport over the African continent. Due to the contribution of the day-to-night contrast of brightness temperatures, which is low over oceans, this method can be applied only over land.

The BMDI is not only capable of the qualitative detection of mineral dust, but also able to reflect atmospheric dust column load, limited by particle size dependence and dust layer height effects. The dust index design has been presented together with a motivation for the observation times included into the BMDI by means of meteorological conditions of dust source activation. As opposed to AOD or other products retrieved from reflected solar radiation, BMDI is not sensitive to smoke aerosols such as from biomass burning. As biomass burning aerosol is a prominent feature especially in the sub-Saharan dry seasons and aerosol plumes often mix or form vertically separated layers within the atmospheric column, BMDI gives the possibility of remote sensing the mineral dust aerosol fraction without contributions of external mixed biomass burning aerosols. This is especially of interest, when aerosol effects such as their influence on cloud properties are in the focus of analysis.

Atmospheric humidity has been shown to be a crucial factor in detecting mineral dust with this IR method. Dust detection capabilities of the BMDI are reduced in scenes with high humidity and the upper bound of water vapour column still allowing dust to be detected with the BMDI varies with the dust load. Thus in areas with high humidity conditions being a prominent feature, dust detection is limited by the water vapour effect. The limitation of BMDI dust detection by water vapour can be regarded as being the same (dust detection only reliable for WVC<3 cm) as for the IDDI technique (Legrand et al., 2001). Mineral dust detection with BMDI is reliable over the Sahara in all seasons, while in the West-African Monsoon area dust is detected mainly in the dry season and BMDI dust detection is limited during the monsoon season. One year of BMDI has been evaluated by comparison with surface observations of eight suitable AERONET stations, MODIS “Deep Blue” AOD and OMI Aerosol Index. The correlation of BMDI and AERONET AOD is quite good with $r = -0.796$. As BMDI is assumed to be height dependent and AERONET AOD also includes contributions of biomass burning aerosol, this correlation indicates that BMDI is suitable for detection of mineral dust and, with some restrictions, also is capable of dust load estimation. AERONET observations show very clearly a limitation of BMDI dust detection in scenes with high water vapour columns. The same conclusions as for AERONET can be drawn from comparisons with MODIS AOD and OMI AI. On the other hand especially the comparison with OMI AI reveals the different and apparently non-linear height dependence of both AI and BMDI. Correlations between MODIS AOD, OMI AI and BMDI show very high magnitudes in the Southern and Western Sahara domain and also in Northern Libya and over the Arabian Peninsula. Low magnitudes of correlations occur along mountain sides and over elevated terrain in the northern Sahara.

Time series of BMDI and cloud cover for 2006 have been analysed for four pre-defined regions, being important dust source regions. Annual cycles of dust load as reported in the literature are represented by BMDI area mean values. Together with the cloud cover information, especially for the Akhdar region in northern Libya the role of cyclonic activity in dust mobilisation over this area can be inferred from the time series. The Akhdar region is important concerning dust export towards the Mediterranean Sea. Also the role of the Bodélé Depression and Western Sahara for the overall dust mobilisation is evident from the time series. The application of BMDI to Southern Africa also will be part of future work with one focus on the special meteorological conditions there and their implications for dust detection with different methods.

Only one year of observations has been analysed and presented here. Thus it cannot be answered, if these observations are really representative for annual cycles of mineral dust. Especially the interannual variability of mineral dust load has to be analysed further in future work. BMDI time series covering the whole period from the start of operational MSG observations in 2004 are planned to be analysed with respect to year-to-year variations in regional atmospheric dust variability.

Acknowledgements

We thank Naif Al-Abbadi, Bernadette Chatenet, Phillippe Goloub, Jean Louis Rajot, Didier Tanré and Rick Wagener and their staff for establishing and maintaining the eight AERONET sites used in this investigation and for providing the observation data. We acknowledge the GES-DISC Interactive. Online Visualization ANd aNalysis Infrastructure (Giovanni) as part of the NASA's Goddard Earth Science (GES) Data and Information Service. Center (DISC) for the OMI AI data set. We thank the MODIS Atmosphere Discipline Group for providing MODIS aerosol data. We also acknowledge the NASA's Goddard Space Flight Center's Level 1 and Atmosphere Archive and Distribution System (LAADS) for the online distribution of the MODIS data.

Furthermore, we acknowledge the U.S. Geological Survey's Earth Resources Observation and Science (EROS) data center for providing the digital elevation data set GTOPO30.

We thank four anonymous reviewers for their very useful comments, which helped improve this manuscript.

References

Ackerman, S. A. (1997). Remote sensing aerosol using satellite infrared observations. *Journal of Geophysical Research*, *102*(D14), 17069−17079.

Alpert, P., & Ziv, B. (1989). The Sharav cyclone — Observations and some theoretical considerations. *Journal of Geophysical Research*, *94*, 18495−18514.

Ansmann, A., Tesche, M., Althausen, D., Müller, D., Seifert, P., Freudenthaler, V., et al. (2008). Influence of Saharan dust on cloud glaciation in southern Morocco during the Saharan Mineral Dust Experiment. *Journal of Geophysical Research*, *113*, D04210. doi:10.1029/2007JD008785.

Banta, R. M., Pichugina, Y. L., & Brewer, W. A. (2006). Turbulent velocity-variance profiles in the stable boundary layer generated by a nocturnal low-level jet. *Journal of the Atmospheric Sciences*, *63*, 2700–2719.

Barkan, J., Alpert, P., Kutiel, H., & Kishcha, P. (2005). Synoptics of dust transportation days from Africa toward Italy and central Europe. *Journal of Geophysical Research*, *110*, D07208. doi:10.1029/2004JD005222.

Blackadar, A. K. (1957). Boundary layer wind maxima and their significance for the growth of nocturnal inversion. *Bulletin of the American Meteorological Society*, *38*, 283–290.

Breitkreuz, H., Schroedter-Homscheidt, M., & Holzer-Popp, T. (2007). A case study to prepare for the utilization of aerosol forecasts in solar energy industries. *Solar Energy*, *81*, 1377–1385.

Brooks, N., & Legrand, M. (2006). Dust variability over northern Africa and rainfall in the Sahel. In S. J. McLaren & D. Kniveton (Eds.), *Linking climate change to land surface change* (pp. 1–25). Dordecht, Netherlands: Kluwer Acad.

Chaboureau, J. -P., Tulet, P., & Mari, C. (2007). Diurnal cycle of dust and cirrus over West Africa as seen from Meteosat Second Generation satellite and a regional forecast model. *Geophysical Research Letters*, *34*, L02882. doi:10.1029/2006GL027771.

Dubovik, O., Holben, B., Eck, T. F., Smirnov, A., Kaufman, Y. J., King, M. D., et al. (2002). Variability of absorption and optical properties of key aerosol types observed in worldwide locations. *Journal of the Atmospheric Sciences*, *59*, 590–608.

Dunion, J. P., & Velden, C. S. (2004). The impact of the Saharan Air Layer on Atlantic tropical cyclone activity. *Bulletin of the American Meteorological Society*, *85*, 353–365.

Engelstaedter, S., Tegen, I., & Washington, R. (2006). North African dust emissions and transport. *Earth-Science Reviews*, *79*, 73–100.

Engelstaedter, S., & Washington, R. (2007). Atmospheric controls on the annual cycle of North African dust. *Journal of Geophysical Research*, *112*, D03103.

Evan, A. T., Dunion, J., Foley, J. A., Heidinger, A. K., & Velden, C. S. (2006). New evidence for a relationship between Atlantic tropical cyclone activity and African dust outbreaks. *Geophysical Research Letters*, *33*, L19813. doi:10.1029/2006GL026408.

Holben, B. N., Eck, T. F., Slutsker, I., Tanre, D., Buis, J. P., Setzer, A., et al. (1998). AERONET – A federated instrument network and data archive for aerosol characterization. *Remote Sensing of Environment*, *66*, 1–16.

Holton, J. R. (1967). The diurnal boundary layer wind oscillation above sloping terrain. *Tellus*, *19*, 199–205.

Holzer-Popp, T., Schroedter-Homscheidt, M., Breitkreuz, H., Martynenko, D., & Klüser, L. (2008). Synergetic aerosol retrieval from SCIAMACHY and AATSR onboard ENVISAT. *Atmospheric Chemistry and Physics*, *8*, 7651–7672.

Hsu, N. C., Tsay, S. C., King, M. D., & Herman, J. R. (2004). Aerosol properties over bright-reflecting source regions. *IEEE Transactions on Geoscience and Remote Sensing*, *42*, 557–569.

Hui, W. J., Cook, B. I., Ravi, S., Fuentes, J. D., & D'Odorico, P. (2008). Dust-rainfall feedbacks in the West African Sahel. *Water Resources Research*, *44*, W05202. doi:10.1029/2008WR006885.

Jickells, T. D., An, Z. S., Andersen, K. K., Baker, A. R., Bergametti, G., Brooks, N., et al. (2005). Global iron connections between desert dust, ocean biogeochemistry, and climate. *Science*, *308*, 67–71.

Kalu, A. E. (1979). The African dust plume: Its characteristics and propagation across west Africa in winter. *SCOPE*, *14*, 95–118.

Kaufman, Y. J., & Fraser, R. S. (1997). The effect of smoke particles on clouds and climate forcing. *Science*, *277*, 1636–1639.

King, M. D., Kaufman, Y. J., Tanré, D., & Nakajima, T. (1999). Remote sensing of tropospheric aerosols from space: Past, present and future. *Bulletin of the American Meteorological Society*, *80*, 2229–2259.

Klüser, L., Rosenfeld, D., Macke, A., & Holzer-Popp, T. (2008). Observations of convective clouds generated by solar heating of dark smoke plumes. *Atmospheric Chemistry and Physics*, *8*, 2833–2840.

Knippertz, P., Ansmann, A., Althausen, D., Müller, D., Tesche, M., Bierwirth, E., et al. (2008). Dust mobilization and transport in the Northern Sahara during SAMUM 2006 – A meteorological overview. *Tellus*, *61B*(1), 12–31. doi:10.1111/j.1600-0889.2008.00380.x.

Koren, I., Kaufman, Y. J., Washington, R., Todd, M. C., Rudich, Y., Martins, J. V., et al. (2006). The Bodélé depression: A single spot in the Sahara that provides most of the mineral dust to the Amazon forest. *Environmental Research Letters*, *1*. doi:10.1088/1748-9326/1/1/014005.

Kriebel, K. T., Gesell, G., Kästner, M., & Mannstein, H. (2003). The cloud analysis tools APOLLO: Improvements and validations. *International journal of remote sensing*, *24*, 2389–2408.

Legrand, M., Plana-Fattori, A., & N'doume, C. (2001). Satellite detection of dust using the IR imagery of Meteosat, 1. Infrared Difference Dust Index. *Journal of Geophysical Research*, *106*(D16), 18251–18274.

Lenschow, D. H., & Stankov, B. (1979). The rapid morning boundary–layer transition. *Journal of the Aeronautical Sciences*, *36*, 2108–2124.

Li, J., Zhang, P., Schmit, T. J., Schmetz, J., & Menzel, W. P. (2007). Quantitative monitoring of a Saharan dust event with SEVIRI on Meteosat-8. *International journal of remote sensing*, *28*, 2181–2186.

Mahowald, N. M., & Kiehl, L. M. (2003). Mineral aerosol and cloud interactions. *Geophysical Research Letters*, *30*, 1475. doi:10.1029/2002GL016762.

Mahowald, N. M., Baker, A. R., Bergametti, G., Brooks, N., Duce, R. A., Jickells, T. D., et al. (2005). Atmospheric global dust cycle and iron inputs to the ocean. *Global Biogeochemical Cycles*, *19*, GB4025. doi:10.1029/2004GB002402.

Marticorena, B., & Bergametti, G. (1995). Modeling the atmospheric dust cycle: 1. Design of a soil-derived dust emission scheme. *Journal of Geophysical Research*, *100*(D8), 16415–16430.

McConnell, C. L., Highwood, E. J., Coe, H., Formenti, P., Anderson, B., Osborne, S., et al. (2008). Seasonal variations of the physical and optical characteristics of Saharan dust: Results from the Dust Outflow and Deposition to the Ocean (DODO) experiment. *Journal of Geophysical Research*, *113*, D14S05. doi:10.1029/2007JD009606.

Meloni, D., di Sarra, A., Biavati, G., DeLuisi, J. J., Montelone, F., Pace, G., et al. (2006). Seasonal behavior of Saharan dust events at the Mediterranean island of Lampedusa in the period 1999–2005. *Atmospheric Environment*, *41*, 3041–3056.

Miller, S. D., Kuciauskas, A. P., Liu, M., Ji, Q., Reid, J. S., Breed, D. W., et al. (2008). Haboob dust storms of the southern Arabian Peninsula. *Journal of Geophysical Research*, *112*, D01202. doi:10.1029/2007JD008550.

Minnis, P., Young, D. F., & Harrison, E. F. (1991). Examination of the relationship between outgoing infrared window and total longwave fluxes using satellite data. *Journal of Climate*, *4*, 1114–1133.

Ogawa, K., Schmugge, T., & Jacob, F. (2003). Estimation of land surface window (8–12 µm) emissivity from multispectral thermal infrared remote sensing —A case study in a part of Sahara desert. *Geophysical Research Letters*, *30*. doi:10.1029/2002GL016354.

Pedgley, D. E. (1972). Desert depression over North-East Africa. *Meteorological Magazine*, *101*, 228–244.

Pierangelo, C., Chedin, A., Heiliette, S., Jacquinet-Husson, N., & Armante, R. (2004). Dust altitude and infrared optical depth from AIRS. *Atmospheric Chemistry and Physics*, *4*, 1813–1822.

Prospero, J. M., & Carlson, T. N. (1980). Saharan Air Outbreaks over the North Atlantic. *Pure and Applied Geophysics*, *119*, 677–691.

Prospero, J. M., Ginoux, P., Torres, O., Nicholson, S. E., & Gill, T. E. (2002). Environmental characterization of global dust sources of atmospheric soil dust identified with the Nimbus 7 Total Ozone Mapping Spectrometer (TOMS) absorbing aerosol product. *Reviews of Geophysics*, *40*, 1002. doi:10.1029/2000RG000095.

Richard, Y., Martiny, N., Fauchereau, N., Reason, C., Rouault, M., Vigaud, N., et al. (2008). Interannual memory effects for spring NDVI in semi-arid South Africa. *Geophysical Research Letters*, *35*, L13704. doi:10.1029/2008GL034119.

Rosenfeld, D., Rudich, Y., & Lahev, R. (2001). Desert dust suppressing precipitation: A possible desertification feedback loop. *PNAS*, *98*, 5975–5980.

Rudich, Y., Sagi, A., & Rosenfeld, D. (2003). Influence of the Kuwait oil fire plume (1991) on the microphysical development of clouds. *Journal of Geophysical Research*, *108*. doi:10.1029/2003JD003472.

Schepanski, K., Tegen, I., Laurent, B., Heinold, B., & Macke, A. (2007). A new Saharan dust source activation frequency map derived from MSG–SEVIRI IR-channels. *Geophysical Research Letters*, *34*, L18803. doi:10.1029/2007GL030168.

Schepanski, K., Tegen, I., & Macke, A. (2009). Saharan Dust Transport and Deposition towards the Tropical Northern Atlantic. *Atmospheric Chemistry and Physics*, *9*, 1173–1189.

Schepanski, K., Tegen, I., Todd, M. C., Heinold, B., Bönisch, G., Laurent, B., et al. (in press). Meteorological processes forcing Saharan dust emission inferred from MSG–SEVIRI observations of sub-daily dust source activation and numerical models. *Journal of Geophysical Research*. doi:10.1029/2008JD010325

Schmetz, J. P., Pili, P., Tjemkes, S., Just, D., Kerkmann, J., Rota, S., et al. (2002). An introduction to Meteosat Second Generation (MSG). *Bulletin of the American Meteorological Society*, *83*, 977–992.

Schroedter-Homscheidt, M., Drews, A., & Heise, S. (2008). Total water vapor column retrieval from MSG–SEVIRI split window measurements exploiting the daily cycle of land surface temperatures. *Remote Sensing of Environment*, *112*, 249–258.

Slingo, A., Ackerman, T. P., Allan, R. P., Kassianov, E. I., McFarlane, S. A., Robinson, G. J., et al. (2006). Observations of the impact of a major Saharan dust storm on the atmospheric radiation balance. *Geophysical Research Letters*, *33*, L24817. doi:10.1029/2006GL027869.

Sokolik, I. N. (2002). The spectral radiative signature of wind-blown mineral dust: Implications for remote sensing in the thermal IR region. *Geophysical Research Letters*, *29*, 2154. doi:10.1029/2002GLR015910.

Spearman, C. (1908). The method of "right and wrong cases" (constant stimuli) without Gauss' formulae. *British Journal of Psychology*, *2*, 227–242.

Todd, M. C., Washington, R., Raghavan, S., Lizcano, G., & Knippertz, P. (2008). Regional model simulations of the Bodélé Low-level Jet of Northern Chad during the Bodélé Dust Experiment (BoDEx 2005). *Journal of Climate*, *21*, 995–1012.

Torres, O., Bhartia, P. K., Herman, J. R., Ahmad, Z., & Gleason, J. (1998). Derivation of aerosol properties from a satellite measurements of backscattered ultraviolet radiation: Theoretical basis. *Journal of Geophysical Research*, *103*, 17099–17110.

Trigo, I. F., Bigg, G. R., & Davies, T. D. (2002). Climatology of cyclogenesis mechanisms in the Mediterranean. *Monthly Weather Review*, *130*, 549–569.

Tulet, P., Mallet, M., Pont, V., Pelon, J., & Boone, A. (2008). The 7–13 March 2006 dust storm over West Africa: Generation, transport and vertical stratification. *Journal of Geophysical Research*, *113*, D00C08. doi:10.1029/2008JD009871.

Wald, A. E., Kaufman, Y. J., Tanré, D., & Gao, B. C. (1998). Daytime and nighttime detection of mineral dust over desert using infrared spectral contrast. *Journal of Geophysical Research*, *103*(D24), 32307–32313.

Washington, R., & Todd, M. C. (2005). Atmospheric controls on mineral dust emission from the Bodélé Depression, Chad: The role of the low level jet. *Geophysical Research Letters*, *32*, L17701. doi:10.1029/2005GL023597.

Washington, R., Todd, M. C., Engelstaedter, S., Mbainayel, S., & Mitchell, F. (2006). Dust and the low-level circulation over the Bodélé Depression, Chad: Observations from BoDEx 2005. *Journal of Geophysical Research*, *111*(D3), 201.

Please cite this article as: Klüser, L., & Schepanski, K., Remote sensing of mineral dust over land with MSG infrared channels: A new Bitemporal Mineral Dust Index, *Remote Sensing of Environment* (2009), doi:10.1016/j.rse.2009.04.012